

การศึกษาแปลกรรมทางด้านข้างของโครงสร้างคอนกรีตเมื่อกระตุ้นด้วยแสง



นางสาวฤดีสันติ ส่องเมือง

สถาบันวิทยบริการ  
วิทยานิพนธ์นี้เป็นส่วนหนึ่งของการศึกษาตามหลักสูตรปริญญาวิศวกรรมศาสตรมหาบัณฑิต  
สาขาวิชาวิศวกรรมไฟฟ้า ภาควิชาวิศวกรรมไฟฟ้า  
คณะวิศวกรรมศาสตร์ จุฬาลงกรณ์มหาวิทยาลัย

ปีการศึกษา 2542

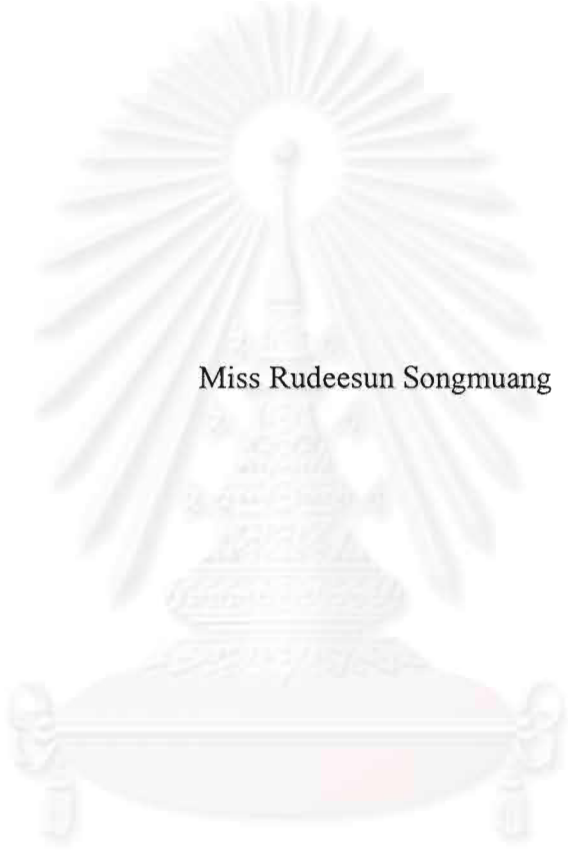
ISBN 974-333-572-2

ลิขสิทธิ์ของจุฬาลงกรณ์มหาวิทยาลัย

1 2 พ.ย. 2546

I 19.265499

**STUDY OF OPTICALLY PUMPED EDGE EMISSION SPECTRA  
FROM QUANTUM STRUCTURE**



Miss Rudeesun Songmuang

A Thesis Submitted in Partial Fulfillment of the Requirements  
for the Degree of Master of Engineering in Electrical Engineering

Department of Electrical Engineering

Faculty of Engineering

Chulalongkorn University


Academic Year 1999

ISBN 974-333-572-2

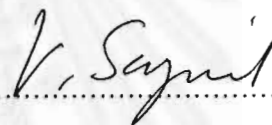
Thesis Title Study of Optically Pumped Edge Emission Spectra from Quantum Structure  
By Miss Rudeesun Songmuang  
Department Electrical Engineering  
Thesis Advisor Professor Dr. Somsak Panyakeow

---

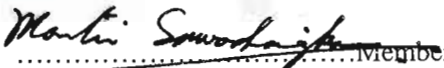
Accepted by the Faculty of Engineering, Chulalongkorn University, in Partial Fulfillment of  
the Requirements for the Master's Degree


  
..... Dean of Faculty of Engineering  
( Professor Dr. Somsak Panyakeow )

Thesis Committee

  
..... Chairman  
(Professor Dr. Virulh Sa-yakanit)

  
..... Thesis Advisor  
(Professor Dr. Somsak Panyakeow)

  
..... Member  
(Associate Professor Dr. Montri Sawadsaringkarn)

  
..... Member  
(Assistant Professor Dr. Somchai Ratanathammaphan)

ฤดีสันต์ ส่องเมือง: การศึกษาสเปกตรัมทางด้านข้างของโครงสร้างควอนตัมเมื่อกระตุ้นด้วยแสง (STUDY OF OPTICALLY PUMPED EDGE EMISSION SPECTRA FROM QUANTUM STRUCTURE) อาจารย์ที่ปรึกษา: ศ.ดร.สมศักดิ์ ปัญญาแก้ว, 61 หน้า, ISBN 974-333-572-2

วิทยานิพนธ์ฉบับนี้ นำเสนอการศึกษาสเปกตรัมของการเปล่งแสงทางด้านข้างของโครงสร้างซิงเกิลควอนตัมเวลล์และมัลติเพิลควอนตัมเวลล์ของสารกึ่งตัวนำชนิดแกลเลียมอาร์เซไนด์/อะลูมิเนียมแกลเลียมอาร์เซไนด์ (ปริมาณอะลูมิเนียมต่อแกลเลียม 20%) และอินเดียมแกลเลียมอาร์เซไนด์/แกลเลียมอาร์เซไนด์ (ปริมาณอินเดียมต่อแกลเลียม 20%) เมื่อได้รับการกระตุ้นด้วยแสงอาร์กอนเลเซอร์ (ความยาวคลื่น 5140 Å) โครงสร้างที่ใช้ในการทดลองสร้างขึ้นด้วยวิธีการปลูกผลึกด้วยลำโมเลกุล จากการศึกษาและการทดลองพบว่า เมื่อโครงสร้างมัลติเพิลควอนตัมเวลล์ได้รับการกระตุ้นด้วยแสงที่มีความเข้มสูง มีแนวโน้มที่จะเปล่งแสงแบบถูกเร่ง ซึ่งเป็นพื้นฐานของการเกิดแสงเลเซอร์ โดยแสงที่เปล่งจากโครงสร้างมัลติเพิลควอนตัมเวลล์ของสารกึ่งตัวนำชนิดแกลเลียมอาร์เซไนด์/อะลูมิเนียมแกลเลียมอาร์เซไนด์นั้น จะมีความเข้มเพิ่มขึ้นอย่างรวดเร็วที่ความเข้มแสงที่ใช้ในการกระตุ้นประมาณ 4 กิโลวัตต์ต่อตารางเซนติเมตรและ 2.5 กิโลวัตต์ต่อตารางเซนติเมตร สำหรับโครงสร้าง 10 มัลติเพิลควอนตัมเวลล์และ 5 มัลติเพิลควอนตัมเวลล์ในโครงสร้างช่องนำคลื่น ตามลำดับ ส่วนแสงที่เปล่งจากโครงสร้าง 3 และ 5 มัลติเพิลควอนตัมเวลล์ของสารกึ่งตัวนำชนิดอินเดียมแกลเลียมอาร์เซไนด์/แกลเลียมอาร์เซไนด์ จะมีความเข้มเพิ่มขึ้นอย่างไม่เชิงเส้นแต่ไม่แสดงจุดเปลี่ยนแปลงที่ชัดเจน เนื่องจากการสูญเสียในชั้นก้ำกีดแสง

ภาควิชา ..... วิศวกรรมไฟฟ้า  
สาขาวิชา ..... วิศวกรรมไฟฟ้า  
ปีการศึกษา ..... 2542

ลายมือชื่อนิสิต ..... ฤดีสันต์ ส่องเมือง  
ลายมือชื่ออาจารย์ที่ปรึกษา ..... *Mercer*  
ลายมือชื่ออาจารย์ที่ปรึกษาพร้อม .....

RUDEESUN SONGMUANG: STUDY OF OPTICALLY PUMPED EDGE  
EMISSION SPECTRA FROM QUANTUM STRUCTURE. THESIS  
ADVISOR: PROF. DR. SOMSAK PANYAKEOW, D. Eng. 61 pp. ISBN  
974-333-572-2

Edge emission spectra of GaAs/Al<sub>0.2</sub>Ga<sub>0.8</sub>As and In<sub>0.2</sub>Ga<sub>0.8</sub>As/GaAs single quantum well and multiple quantum well were investigated by optically-pumped technique using argon laser (5140 Å). The structures were grown by the molecular beam epitaxial technique. Multiple quantum wells fabricated from both material systems show the possibility of stimulated emission which is the fundamental of laser action. In Al<sub>0.2</sub>Ga<sub>0.8</sub>As/GaAs case, rapid increase of edge emission from 10 multiple quantum well and 5 multiple quantum well with waveguide structures were observed when the pumping intensity reached a threshold values of ~ 4 kW/cm<sup>2</sup> and 2.5 kW/cm<sup>2</sup>, respectively. The spectra from In<sub>0.2</sub>Ga<sub>0.8</sub>As/GaAs 3 and 5 multiple quantum well structures showed the superlinear increase; however, the threshold pumping intensity was not clearly observed as a result of losses in the active region of these structures.

ภาควิชา ..... วิศวกรรมไฟฟ้า .....  
สาขาวิชา ..... วิศวกรรมไฟฟ้า .....  
ปีการศึกษา ..... 2542 .....

ลายมือชื่อนิสิต ..... ด.ญ. สันติ ..... ส.อ.ง.บ.ร.จ. ....  
ลายมือชื่ออาจารย์ที่ปรึกษา ..... *Alu de* .....  
ลายมือชื่ออาจารย์ที่ปรึกษาร่วม .....

## ACKNOWLEDGEMENT

The author would like to give a special thanks to my parents for their supports.

The author gratefully acknowledges all those who provided invaluable help and encouragement during researching and writing this thesis at the Semiconductor Device Research Laboratory (SDRL), Department of Electrical Engineering, Faculty of Engineering, Chulalongkorn University. In particular, the author is deeply indebted to Professor Dr. Somsak Panyakeow, who is the advisor, Dr. Karl Eberl, Professor Dr. Ignaz Eisele, Associate Professor Dr. Montri Sawadsaringkarn, Associate Professor Dr. Choopol Antarasena, and Assistant Professor Dr. Somchai Ratanathammaphan.

As always, this thesis could not have been completed without special concern of staffs in SDRL, Dr. Suwat Sopitpan, Mr. Supachok and Mrs. Kwanruan Thainoi, Mr. Pornchai Changmoung. In addition, I would like to thank for recommendation on my works by Dr. Songphol Kanjanachuchai, Dr. Arporn Teeramongkonradsame, Mr. Nutchai Sroymadee, and Mr. Suwit Kiravittaya.

Special thanks are due to the Sit Kon Kuti scholarship for the fund for research and the sandwiched program at Universität der Bundeswher München, Germany. I am grateful to Associate Professor Dr. Anuvat Sirivat and the Petroleum and Petrochemical College for providing the high power argon laser. Finally, I would like to acknowledge the Japan International Cooperation Agency (JICA) for providing the molecular beam epitaxy machine and accessories for doing this research.

สถาบันวิทยบริการ  
จุฬาลงกรณ์มหาวิทยาลัย

# CONTENTS

	Page
Abstract (Thai) .....	iv
Abstract (English) .....	v
Acknowledgment .....	vi
Contents .....	vii
List of Figures .....	ix
List of Table .....	xii
CHAPTER	
1 Introduction .....	1
1.1 Background .....	1
1.2 Objective .....	4
1.3 Overview .....	4
2 Basic of Quantum Well Structure .....	5
2.1 Introduction .....	5
2.2 Fundamental .....	5
2.3 2-D density of states .....	9
2.4 Strained quantum well .....	10
2.5 Calculation result of GaAs/Al <sub>x</sub> Ga <sub>1-x</sub> As quantum well .....	12
2.6 Calculation result of In <sub>x</sub> Ga <sub>1-x</sub> As/GaAs strained quantum well ...	15
3. Optical gain in quantum well structure .....	18
3.1 Introduction .....	18
3.2 Slab waveguide .....	18
3.3 Optical gain .....	22
3.4 Modal gain .....	30
4. Fabrication and Measurement Technique .....	31
4.1 Fabrication process .....	31
4.1.1 Substrate preparation .....	31
4.1.2 The flux calibration .....	31
4.1.3 Growth process .....	32



## CONTENTS (continued)

4.1.4	Optical cavity fabrication .....	37
4.2	Measurement setup .....	38
4.2.1	Photoluminescence measurement .....	38
4.2.2	Optically pumped measurement .....	39
4.3	Conclusion .....	40
5.	Result and Discussion .....	41
5.1	Introduction .....	41
5.2	Photoluminescence .....	41
5.3	Optically pump .....	47
5.3.1	GaAs /Al <sub>0.2</sub> Ga <sub>0.8</sub> As quantum well structures ...	47
5.3.2	In <sub>0.2</sub> Ga <sub>0.8</sub> As/GaAs quantum well structures ....	50
5.3.2	Comparison for 2 systems .....	52
6.	Conclusion .....	53
References	.....	54
Appendix A	.....	58
List of publication	.....	60
Biography	.....	61



## LIST OF FIGURES

Figures	Page
1.1	State-of-art GaAs laser diode threshold current density during first to years (1965-1975) ..... 2
1.2	RIBER 32P MBE system at Chulalongkorn University ..... 3
2.1	Illustration of a quantum-well potential and the corresponding lowest energy carrier wavefunction ..... 6
2.2	$E-k$ relation in $x-y$ direction of QW structure ..... 7
2.3	The potential for wavefunction calculation ..... 8
2.4	Density of states of quantum well and bulk ..... 9
2.5	The critical thickness of $\text{In}_x\text{Ga}_{1-x}\text{As}$ on GaAs system ..... 10
2.6	(a) The tensile strain layer, (b) The lattice-matched layer, and (c) The compressive strain layer ..... 11
2.7	Schematic band representation in strained layers under tensile (a) and compressive (c) strain along with the unstrained case (b) as the reference ..... 11
2.8	The quantized energy level of GaAs/ $\text{Al}_{0.1}\text{Ga}_{0.9}\text{As}$ quantum well ..... 13
2.9	The quantized energy level of GaAs/ $\text{Al}_{0.2}\text{Ga}_{0.8}\text{As}$ quantum well ..... 13
2.10	The quantized energy level of GaAs/ $\text{Al}_{0.3}\text{Ga}_{0.7}\text{As}$ quantum well..... 14
2.11	The quantized energy level of GaAs/ $\text{Al}_{0.4}\text{Ga}_{0.6}\text{As}$ quantum well..... 14
2.12	The quantized energy level of $\text{In}_{0.05}\text{Ga}_{0.95}\text{As}/\text{GaAs}$ strained quantum well ..... 15
2.13	The quantized energy level of $\text{In}_{0.10}\text{Ga}_{0.90}\text{As}/\text{GaAs}$ strained quantum well ..... 16
2.14	The quantized energy level of $\text{In}_{0.15}\text{Ga}_{0.85}\text{As}/\text{GaAs}$ strained quantum well ..... 16
2.15	The quantized energy level of $\text{In}_{0.20}\text{Ga}_{0.80}\text{As}/\text{GaAs}$ strained quantum well ..... 17
3.1	The one dimension slab waveguide..... 18
3.2	The calculated confinement factor for the GaAs/ $\text{Al}_{0.2}\text{Ga}_{0.8}\text{As}$ double heterostructure. The inset shows the expand view in the quantum size region..... 21
3.3	The confinement factor of GaAs/ $\text{Al}_{0.2}\text{Ga}_{0.8}\text{As}$ multiple quantum well with 100 Å well width and 300 Å barrier..... 21
3.4	The function $(E - E_g)^{\frac{1}{2}} (f(E^e) + f(E^h) - 1)$ of bulk GaAs at 77 K for bulk carrier densities $4 \times 10^{18}$ , $6 \times 10^{18}$ , and $8 \times 10^{18} \text{ cm}^{-3}$ ..... 24

## LIST OF FIGURES (continued)

3.5	The function $(E - E_g)^{\frac{1}{2}}(f(E^e) + f(E^h) - 1)$ of bulk GaAs at 300 K for bulk carrier densities $4 \times 10^{18}$ , $6 \times 10^{18}$ , and $8 \times 10^{18} \text{ cm}^{-3}$ .....	25
3.6	The function $f(E^e) + f(E^h) - 1$ of GaAs/Al <sub>0.2</sub> Ga <sub>0.8</sub> As quantum well with 100 Å well width at 300 K for sheet carrier densities $4 \times 10^{12}$ , $6 \times 10^{12}$ , and $8 \times 10^{12} \text{ cm}^{-2}$ .....	25
3.7	The function $f(E^e) + f(E^h) - 1$ of GaAs/Al <sub>0.2</sub> Ga <sub>0.8</sub> As quantum well with 100 Å well width at 300 K for sheet carrier densities $4 \times 10^{12}$ , $6 \times 10^{12}$ , and $8 \times 10^{12} \text{ cm}^{-2}$ .....	26
3.8	The function $f(E^e) + f(E^h) - 1$ of In <sub>0.2</sub> Ga <sub>0.8</sub> As/GaAs quantum well with 75 Å well width at 77 K for sheet carrier densities $4 \times 10^{12}$ , $6 \times 10^{12}$ , and $8 \times 10^{12} \text{ cm}^{-2}$ .....	27
3.9	The function $f(E^e) + f(E^h) - 1$ of In <sub>0.2</sub> Ga <sub>0.8</sub> As/GaAs quantum well with 75 Å well width at 300 K for sheet carrier densities $4 \times 10^{12}$ , $6 \times 10^{12}$ , and $8 \times 10^{12} \text{ cm}^{-2}$ .....	27
3.10	The maximum gain shape, $f_{e,c}(n) - f_{e,v}(n)$ , of GaAs/Al <sub>0.2</sub> Ga <sub>0.8</sub> As single quantum well with <b>100 Å well width as a function</b> of carrier density ( $n$ ).....	29
3.11	The maximum gain shape, $f_{e,c}(n) - f_{e,v}(n)$ , of In <sub>0.2</sub> Ga <sub>0.8</sub> As/GaAs strained single quantum well with 75 Å well width as a function of carrier density ( $n$ ).....	29
3.12	The modal gain shape, $\Gamma \cdot (f_{e,c}(n) - f_{e,v}(n))$ , of GaAs/Al <sub>0.2</sub> Ga <sub>0.8</sub> As quantum wells with 100 Å well width as a function of carrier density ( $n$ ).....	30
4.1	The structure designed for gallium flux calibration .....	32
4.2	Examples of RHEED pattern of GaAs substrate.....	33
4.3	GaAs/Al <sub>0.2</sub> Ga <sub>0.8</sub> As quantum well samples represented for lattice matched system (a) GaAs/Al <sub>0.2</sub> Ga <sub>0.8</sub> As SQW, (b) GaAs/Al <sub>0.2</sub> Ga <sub>0.8</sub> As 10 MQW, and (c) GaAs/Al <sub>0.2</sub> Ga <sub>0.8</sub> As 5 MQW with waveguide .....	35
4.4	In <sub>0.2</sub> Ga <sub>0.8</sub> As/GaAs quantum well samples represented for lattice mismatched System (a) In <sub>0.2</sub> Ga <sub>0.8</sub> As/GaAs SQW, (b) In <sub>0.2</sub> Ga <sub>0.8</sub> As/GaAs 3 MQW, and (c) In <sub>0.2</sub> Ga <sub>0.8</sub> As/GaAs 5 MQW .....	36
4.5	Optical cavity fabrication process.....	37

## LIST OF FIGURES (continued)

4.6	Photoluminescence measurement set up.....	39
4.7	Size view edge emission optically pumped measurement.....	40
4.8	The process in this experiment.....	40
5.1	Photoluminescence spectrum from $\text{In}_{0.2}\text{Ga}_{0.8}\text{As}/\text{GaAs}$ 3 MQW with 75 Å well width at 77 K.....	42
5.2	Photoluminescence spectrum from $\text{GaAs}/\text{Al}_x\text{Ga}_{1-x}\text{As}$ quantum well structures.....	42
5.3	Photoluminescence spectrum from $\text{In}_{0.2}\text{Ga}_{0.8}\text{As}/\text{GaAs}$ quantum well structures at 77 K.....	45
5.4	$\text{GaAs}/\text{Al}_{0.2}\text{Ga}_{0.8}\text{As}$ SQW (a) The variation of the maximum intensity with various pumping power. (b) The side view spectra at 2.6 and 7.6 $\text{kW}/\text{cm}^2$ .....	47
5.5	$\text{GaAs}/\text{Al}_{0.2}\text{Ga}_{0.8}\text{As}$ 10MQW (a) The variation of the maximum intensity with various pumping power. (b) The side view spectra at 2.6 and 7.6 $\text{kW}/\text{cm}^2$ .....	48
5.6	$\text{GaAs}/\text{Al}_{0.2}\text{Ga}_{0.8}\text{As}$ 5 MQW with waveguide (a) The variation of the maximum intensity with various pumping power. (b) The side view spectra at 1.3 and 5.1 $\text{kW}/\text{cm}^2$ .....	49
5.7	$\text{In}_{0.2}\text{Ga}_{0.8}\text{As}/\text{GaAs}$ SQW (a) The variation of the maximum intensity with various pumping power. (b) The side view spectra at 1.3 and 7.6 $\text{kW}/\text{cm}^2$ .....	50
5.8	$\text{In}_{0.2}\text{Ga}_{0.8}\text{As}/\text{GaAs}$ 3 MQW (a) The variation of the maximum intensity with various pumping power. (b) The side view spectra at 1.3 and 7.6 $\text{kW}/\text{cm}^2$ .....	51
5.9	$\text{In}_{0.2}\text{Ga}_{0.8}\text{As}/\text{GaAs}$ 5 MQW (a) The variation of the maximum intensity with various pumping power. (b) The side view spectra at 1.3 and 7.6 $\text{kW}/\text{cm}^2$ .....	51

## LIST OF TABLES

Table		Page
2.1	Density of States for Bulk (3D) and Quantum Well (2D) material.....	9
4.1	The flux pressure with corresponding calculated growth rate.....	32
5.1	The FWHM of photoluminescence spectrum from $\text{Al}_{0.2}\text{Ga}_{0.8}\text{As}/\text{GaAs}$ quantum well structure at 77 K.....	43
5.2	Comparison between calculation and experiment result of $\text{Al}_{0.2}\text{Ga}_{0.8}\text{As}/\text{GaAs}$ SQW and MQW at 77 K and 70 K.....	43
5.3	The FWHM of photoluminescence spectra from $\text{GaAs}/\text{In}_{0.2}\text{Ga}_{0.8}\text{As}$ quantum well structure at 77 K.....	45
5.4	Comparison between calculation and experiment result of $\text{GaAs}/\text{In}_{0.2}\text{Ga}_{0.8}\text{As}$ SQW and MQW at 77 K.....	46





# CHAPTER 1

## Introduction



### 1.1 Background

The principle of semiconductor laser is like any solid state lasers, which need a population inversion condition and an optical feedback mechanism to produce laser emission. However, the laser action in semiconductor is different from 2 or 3 level system because lasing in semiconductor occurs in the **band** system. Therefore, the concept of population inversion in semiconductor should first be understood.

When electrons are injected into the active region, they would recombine spontaneously with holes in the valence band and emit photons with energy  $h\nu > E_g$ , where  $h$  is the Planck constant,  $\nu$  is the photon frequency, and  $E_g$  is the energy gap of the semiconductor which makes up the active region. Photons travelling along the active layer would have two types of interactions within the material. First, if the photon energy is greater than the band gap, electrons in the valence band absorb the photons and then are transferred to the conduction band. The second interaction is the reverse process of the first: the photons would initiate excess electrons from the conduction band to the valence band and produce the emission of another identical photon. The latter process is called **stimulated emission**. If the stimulated emission process occurs with a higher rate than the combination of the absorption and the spontaneous emission processes, the optical gain is positive value. To achieve the optical gain, the population inversion should be induced first. The basic condition for population inversion is that **the probability of finding electrons in the upper energy level is greater than the probability of finding them in the lower energy level**. This condition can be expressed by the inequality:

$$F_n - F_p > E_g \quad (1.1)$$

where  $E_{fn}$  and  $E_{fp}$  are the quasi-Fermi (Imref) levels of the conduction and the valence band respectively, and  $E_g$  is the energy gap of the material. When this condition is satisfied, such as in the Fabry-Perot cavity, selective amplification is occurred.

The first experimental prove for this principle was carried out in GaAs material in 1962 [1]. The device, based on GaAs, was consisted of a p-n junction (called **homojunction**) for carrier injection and polished-facets, to provide the optical feedback.

However, this early structure yielded a large threshold current density ( $J_{th} > 50 \text{ kA/cm}^2$ ) at room temperature and its reliability was uncertain [2]. Thus, these laser diodes could not operate at room temperature.

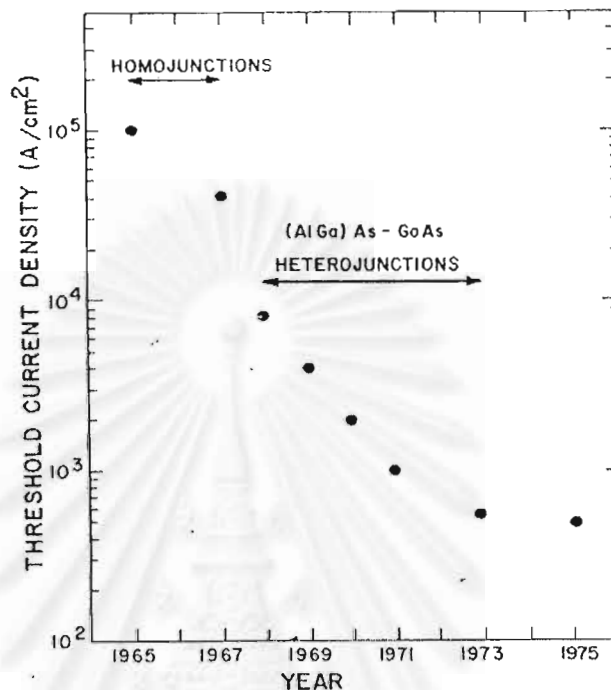


**Fig. 1.1** State-of-art GaAs laser diode threshold current density during first to years (1965-1975) [2]

To improve the efficiency of semiconductor lasers, a **double heterojunction**, (one semiconductor material sandwiched between two higher energy gap cladding layers) was proposed and a pulsed-mode lasing operation at room temperature was reported in 1969 [1]. Since then, the value of threshold current density was continuously improved and the GaAs/AlGaAs laser with  $J_{th} \sim 1.6 \text{ kA/cm}^2$  was demonstrated in 1970 [1]. The reasons for the reduction of threshold current density of the heterostructure laser (see Fig. 1.1) are twofold. First, the cladding layers, which have a large band gap, improve the confinements of electrons and holes in the active layer so they can recombine more efficiently. Second, the higher energy gap materials usually have a high refractive index, which can confine the photons in the active region; the internal loss is thus reduced [1-2]. The electrical and optical confinements result in the greater optical gain.

In the same decades, there was an invention of the precise fabrication technique called Molecular Beam Epitaxy (MBE) [3], which requires an ultra-high vacuum environment. Layers are grown via the reaction between molecular beam and the substrate

surface whose temperature is maintained during growth. Because of the slow growth rate of the MBE process (typically 1  $\mu\text{m}/\text{hour}$ ), the thickness of the growth layer can be controlled precisely and the surface migration of impinging species on the substrate surface is ensured. Thus, the surface of the film after growth film is atomically smooth.

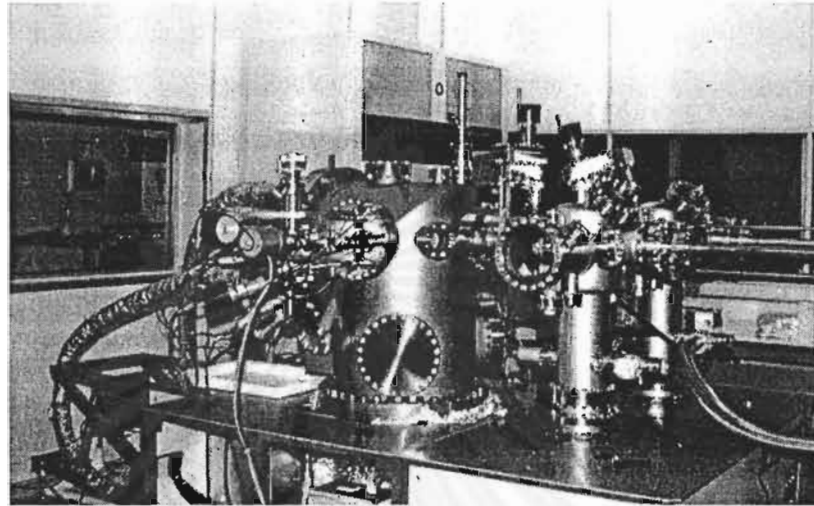


**Fig. 1.2** RIBER 32P MBE system at Chulalongkorn University

Owing to the MBE technique, the active layer of the double heterojunction can be reduced from 0.1-0.2  $\mu\text{m}$  to 50-100  $\text{\AA}$  and causes the confinement of the carriers, in the direction normal to the growth direction. As a result, the kinetic energy of the carriers is quantized into discrete levels. Lasers having this quantum structure as an active region are called **quantum well lasers** (QW laser). The quantum-sized effect gives QW laser many benefits over the conventional laser with bulk active layer such as the ability to tune the photon wavelength by changing the well width [1,4], the resultant lower threshold current density caused by a higher optical gain [1,4], the smaller temperature dependence [5], and the narrower spectrum linewidth caused by lower internal loss and smaller refractive index change under high excitation [4].

At the beginning state of development, most QW lasers were made from GaAs and AlGaAs, which are lattice matched. Both materials have the same lattice constant so the growth layer normally has few dislocations. Later on, the growth of lattice-mismatched system, such as InGaAs/GaAs, was achieved. The epilayers are pseudomorphic and, despite the strain, are defect-free. Strained QW lasers give a better control over the optical polarization. Furthermore, the strain in the QW causes the reduction of the effective hole



mass, so the carrier density needed for population inversion is lower. Therefore, strained QW laser yield lower threshold current [6].

In this chapter, the developments and the benefits of various semiconductor lasers are reviewed. Most semiconductor lasers were operated by current injection. Besides which, there are two other methods of excitation [7-8]:

1. Electroluminescence
2. Photoluminescence or optically pumped.

The **optically pumped** method is the convenient way to study lasing action in semiconductor lasers [7-15] because it does not require the p-n junction. Laser source is especially useful as the optical pump source owing to the high intensity and the finely focused beam [7-8]. However the problem in the optically pumped method is that the penetration depth of a direct gap material is shallow ( $< 1 \mu\text{m}$ ). Despite this limitation, the optically pumped method is still useful for studying lasing action in semiconductor.

## 1.2 Objective

The quantum well structures, as the active layer of the laser in our experiment, are grown by the MBE system at Chulalongkorn University (Fig. 1.2). The optically pumped method, as opposed to the current injection technique, is selected in order to eliminate the preparation of p-n junctions. The variations of the maximum output intensity from these structures with pumping power are studied. The data obtained are useful for designing active layers of the laser diodes.

## 1.3 Overview

This thesis is divided into 4 parts: basic theory, experimental technique, results and discussions and conclusions. The basic theory part consists of 2 chapters: basic theory of quantum well structure in chapter 2 and optical gain in quantum well structure in chapter 3. In the theoretical part, the calculations of quantized states are only in approximation. The experiment part is presented in chapter 4, which gives the details of the fabrication and the measurement set up. The experiment results are reported and discussed in chapter 5. Finally, conclusions are given in chapter 6.

## CHAPTER 2

### Basic of Quantum Well Structure

#### 2.1 Introduction

When the size of semiconductor is reduced to  $< 150 \text{ \AA}$  (comparable to de Broglie wavelength), **quantum size effects** become important and alter electric and optical properties of material. Of particular interest are **quantum wells (QW)**, formed by a sandwich structure of two heterojunction with a very thin active region in between. Due to quantum confinements, the kinetic energy of carriers in the direction normal to the heterointerface is quantized while it is like that of “free” carriers in the in-plane direction,

This chapter provides the basis for the understanding of carrier behaviors in quantum well structures in order to understand the electronic and optical properties of the heterostructures. This chapters also shows the calculations of the quantized energy levels and corresponding emitted photon wavelength of GaAs/AlGaAs and InGaAs/GaAs quantum well structures.

#### 2.2 Wavefunction in quantum wells

To understand carrier (electron and hole) behaviors in quantum well structures, the wavefunction,  $\psi(\mathbf{r})$ , should be examined by solving the Schrödinger equation which equation relates the Hamiltonian  $H_0$  of the crystal lattice to the energy  $E$  of the carriers as stated in eq. (2.1)

$$\begin{aligned} H_0\psi(\mathbf{r}) &= \left( -\frac{\hbar^2}{2m} p^2 + V(\mathbf{r}) \right) \psi(\mathbf{r}) = E\psi(\mathbf{r}) \\ &= \left( -\frac{\hbar^2}{2m} \nabla^2 + V(\mathbf{r}) \right) \psi(\mathbf{r}) = E\psi(\mathbf{r}) \end{aligned} \quad (2.1)$$

where  $\hbar = \frac{h}{2\pi}$ ,  $h$  is Planck's constant,  $m$  is the carrier mass and  $V(\mathbf{r})$  is the lattice potential energy.

The exact solution for the wavefunction  $\psi(\mathbf{r})$  of carriers in the potential well is inconvenient to work with. Fortunately, a simplified model called **the envelope function approximation** has been developed[16]. This model decomposes the crystal potential into

2 parts: periodic atomic-scale potential which is related to the crystal lattice, and macroscopic potential with barrier height determined from the types of semiconductors forming the heterojunctions. The approximation is illustrated in Fig. 2.1.

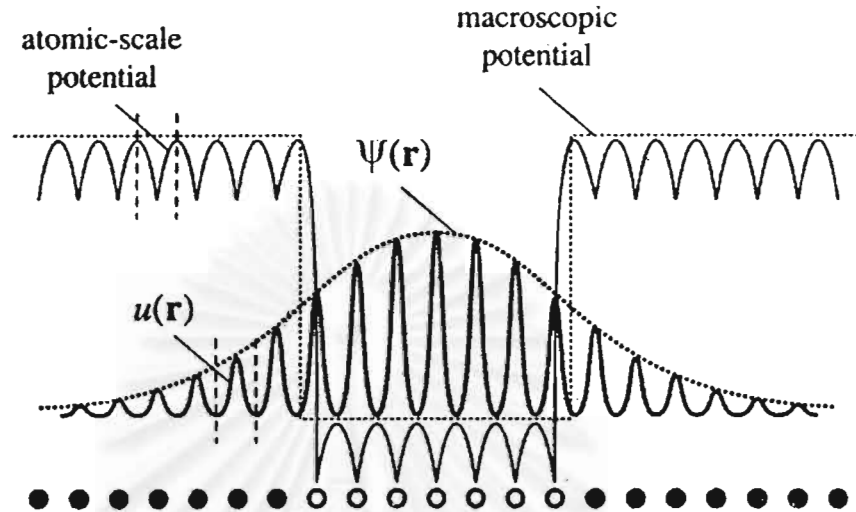


**Fig. 2.1** Illustration of a quantum-well potential and the corresponding lowest energy carrier wavefunction [16]

Therefore, the carrier wavefunction can be written as the product of:

$$\Psi(\mathbf{r}) = \psi(\mathbf{r}) \cdot u(\mathbf{r}) \quad (2.2)$$

$\psi(\mathbf{r})$  and  $u(\mathbf{r})$  are referred to the **envelope** and **Bloch** functions, respectively; they satisfy the Schrödinger equation with macroscopic potential and atomic scale potential boundary conditions.

For a non-degenerate band (excluding spin) such as a conduction band, we can realize the carrier behavior by calculating only the envelope function and include the effect of the periodic atomic potential by using the **effective mass** ( $m^*$ ) instead of the free carrier mass ( $m$ ). For the valence band of a typical III-V compound semiconductor, which is a degenerate system, there is a split between the light hole and the heavy hole bands due to the **spin-orbit coupling effect** [17]. The envelope functions of the heavy and light holes can be separately determined by using different effective masses at  $k = 0$ ,  $m_{hh}^*$  and  $m_{lh}^*$ .

The solution for electron wavefunction in the potential well can thus be calculated as the 'particle in a box' problem in general quantum mechanic textbooks e.g. ref. [18-19].

Due to electron confinements in the direction normal to the interface, the  $z$  direction, the energy levels in this direction are quantized. In the other  $x$  and  $y$  directions, however, the  $E-k$  relation is parabolic, see Fig. 2.2. By using the separation of variables technique, the carrier wavefunction can be written in the following form:

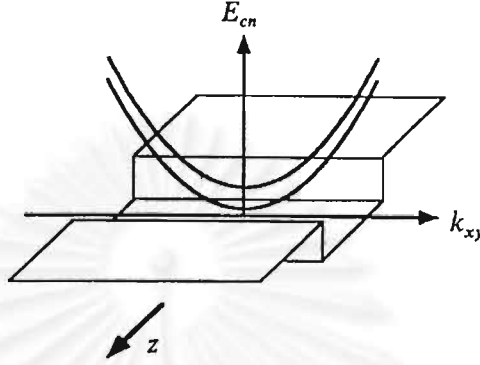


Fig. 2.2  $E-k$  relation in  $x-y$  direction of quantum well structure [20]

$$\psi(\mathbf{r}) = \psi(x)\psi(y)\psi(z) \quad (2.3)$$

and the solutions for carrier wavefunctions in the  $x$  and  $y$  directions are

$$\psi(x) = C_x e^{ik_x x}, \quad \psi(y) = C_y e^{ik_y y} \quad (2.4)$$

which are travelling plane wave as in bulk semiconductors. The wavefunction in the  $z$  direction  $\psi(z)$  can be evaluated by solving the 1 dimension Schrödinger equation as written below

$$\left( -\frac{\hbar^2}{2m^*} \frac{\partial^2}{\partial z^2} + V(z) \right) \psi(z) = E\psi(z) \quad (2.5)$$

where  $V(z)$  is the band discontinuity potential as shown in Fig. 2.3. The solutions of the lowest energy level wavefunction of the equation above is

$$\psi_1(z) = \begin{cases} B \exp\left[ K_2 \left( z + \frac{L}{2} \right) \right] & z < -\frac{L}{2} \\ A \cos K_1 z & |z| \leq \frac{L}{2} \\ B \exp\left[ -K_2 \left( z - \frac{L}{2} \right) \right] & z > \frac{L}{2} \end{cases} \quad (2.6)$$

where

$$K_1 = \sqrt{2m_w^* \frac{E_1}{\hbar^2}}, \quad K_2 = \sqrt{2m_b^* \frac{(V_0 - E_1)}{\hbar^2}},$$

$m_w^*$  and  $m_b^*$  are the electron effective masses in the quantum well and the barrier regions, respectively.

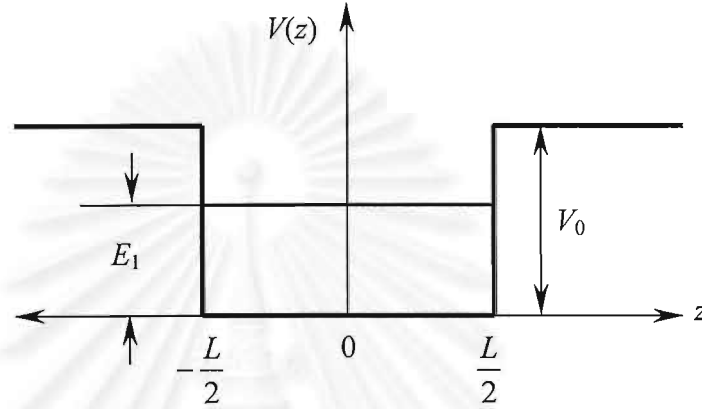


**Fig. 2.3** The potential for wavefunction calculation

From the continuity condition,  $\psi_1(z)$  and  $\frac{1}{m^*} \frac{d\psi_1(z)}{dz}$  must be continuous at the interface. We get

$$\frac{K_1}{m_w^*} \tan\left(\frac{K_1 L}{2}\right) = \frac{K_2}{m_b^*} \quad (2.7)$$

This equation can be solved numerically or graphically and the solution gives information about the lowest quantized state  $E_1$  which governs the optical properties of the quantum well structures.

If the number of wells are increased and the barriers between adjoining wells are thick enough ( $> 50 \text{ \AA}$ ) [21], individual wells are largely uncoupled and the properties of multiple quantum well (MQW) and single quantum well (SQW) are quite similar.

### 2.3 2-D density of states

Another important parameter of quantum well structures is the carrier density of states (DOS). Owing to the one dimension confinement of carrier motion, the 2-D density

of states is independent of energy while the bulk density of states increases with  $\sqrt{E}$ , see Table 2.1 and Fig.2.4. The calculation for density of states can be found in several solid state textbooks [17,19,21-22].

**Table 2.1** Electronic density of States for bulk (3D) and quantum Well (2D) materials

$m$ Dimension	$V_k$	$\frac{dV_k}{dk}$	$\rho(k)$	$\rho(E)^a$
3D	$\frac{4}{3}\pi k^3$	$4\pi k^2$	$\frac{k^2}{\pi^2}$	$\frac{\sqrt{E}}{2\pi^2} \left( \frac{2m^*}{\hbar^2} \right)^{\frac{3}{2}}$
2D	$\pi k^2$	$2\pi k$	$\frac{k}{\pi} \left( \frac{1}{L_z} \right)$	$\frac{m^*}{\pi\hbar^2} \left( \frac{1}{L_z} \right)$

<sup>a</sup> Assuming parabolic bands

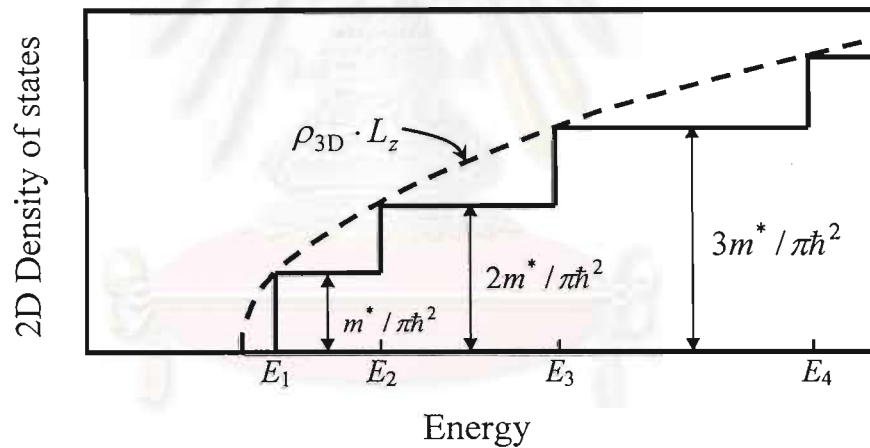


**Fig. 2.4** Density of states in quantum well and in bulk (dashed line)

In a multiple quantum well structure, the density of states can be modified from the single quantum well density of states according to:

$$\rho_{MQW}(E) = n\rho_{SQW}(E) \quad (2.8)$$

where  $n$  is the number of wells in the multiple quantum wells structure.

Due to the step-like nature of 2-D density of states, the efficiency of radiative recombination is improved and is important to laser operation.



## 2.4 Strained quantum well

Due to advances in fabrication techniques, the growth of lattice-mismatched semiconductors with low levels of defects is possible. The growth of lattice-mismatched layer results in the strain in the epi-layer provided that the thickness of the epitaxial layer is below the **critical thickness** (see Fig.2.5).

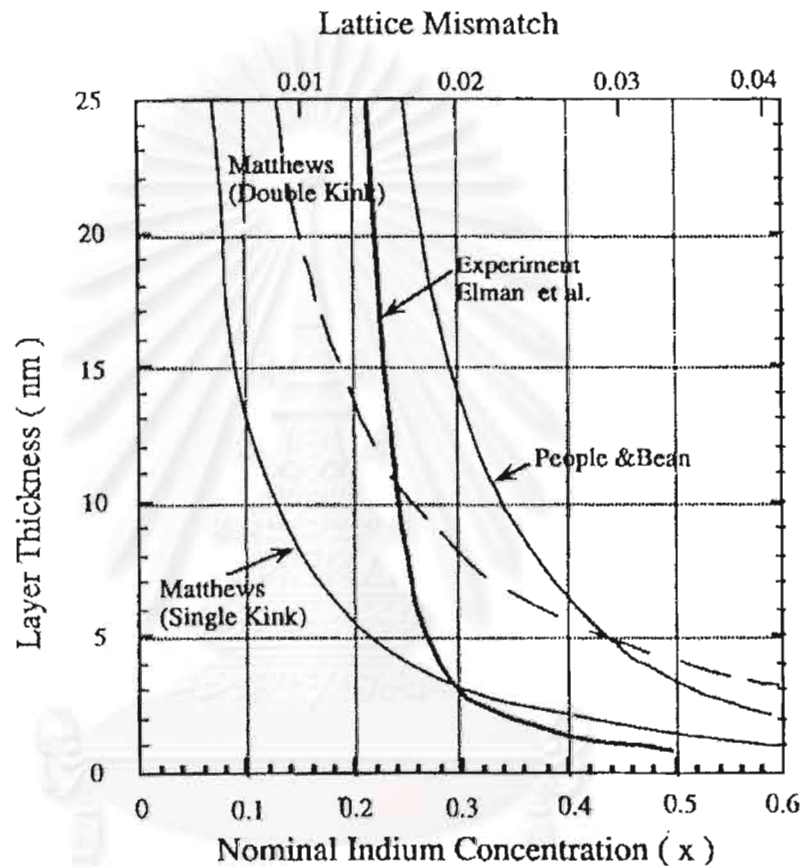


Fig 2.5 The critical thickness of  $\text{In}_x\text{Ga}_{1-x}\text{As}$  on GaAs system [6]

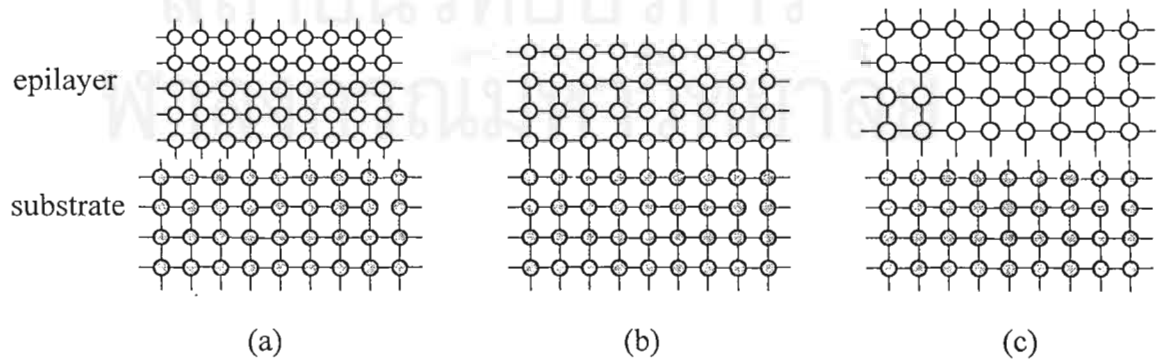
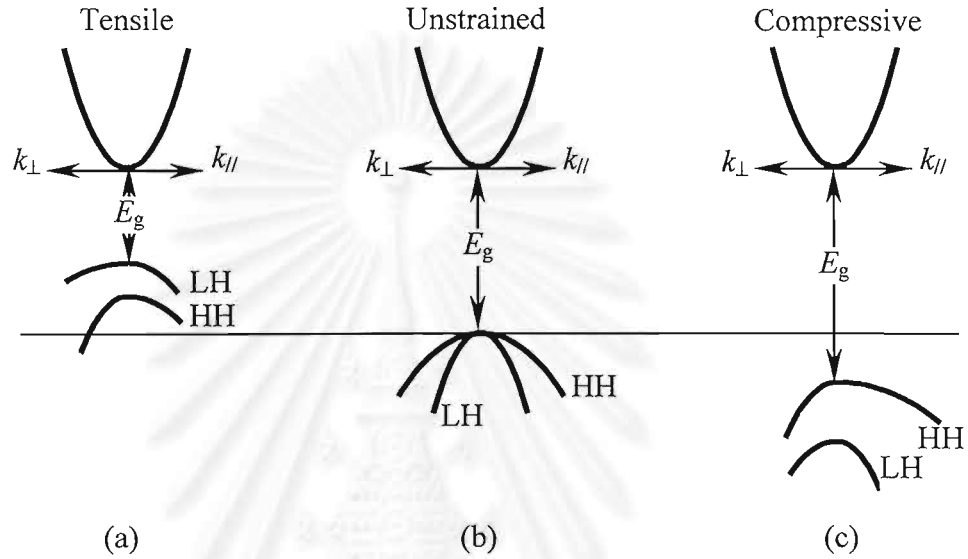


Fig. 2.6 The epilayer (a) under tensile strain, (c) under compressive strain and (b) the lattice-matched to the substrate



If the lattice constant of the growth layer is larger than that of the substrate, e.g.  $\text{In}_x\text{Ga}_{1-x}\text{As}$  on  $\text{InP}$  with  $x < 0.53$  and  $\text{In}_x\text{Ga}_{1-x}\text{As}$  on  $\text{GaAs}$ , **compressive strain** is introduced in the growth layer. Conversely, if the lattice constant of the substrate is larger, e.g.  $\text{In}_x\text{Ga}_{1-x}\text{As}$  on  $\text{InP}$  with  $x > 0.53$ , **tensile strain** is presented in the growth layer. These two cases are depicted in Fig.2.6.



**Fig. 2.7** Schematic band representation in strained layers under tensile (a) and compressive (c) strain along with the unstrained case (b), [6]

Energy bands depend on the lattice structure, when strains are presented. They modified the band structures. The effect of strains on the conduction band of III-V compound semiconductor can be neglected because the band is non-degenerate and spherical in nature [17, 20]. On the other hand, strain distorts the degenerate valence band and splits the light hole band from the heavy hole band as shown in Fig. 2.7. The strained band gap for compressive strain,  $E_{g,strained,compressive}$ , can be written as

$$E_{g,strained,compressive} = E_{g,unstrained} + \delta\epsilon_H \pm \delta\epsilon_s \quad (2.9)$$

where  $E_{g,unstrained}$  is the unstrained band gap,  $\delta\epsilon_H$  is the shift resulted from the hydrostatic component of the strain (positive for compressive and negative for tensile strain), and

$\pm \delta\varepsilon_s$  is the shift originated from the shear component of the strain (for compressive strain, the positive sign is for  $E_g(LH)$  and the negative sign is for  $E_g(HH)$ ).

In a strained quantum well, the energy band especially the valence band is affected not only by quantum effects but also by strains. As mentioned earlier, quantum effects cause the heavy hole and light hole band splitting. When strains are presented, the two bands would move closer (apart) under the tensile (compressive) strain. The light hole and heavy hole would see the different well depth. In compressive strain, the well depth for the light hole is increased (the details of the calculation for light hole band are shown in ref. [20].) and the all LH quantized energy levels further up in the well. In this thesis, we are interested only in the first heavy hole band in  $\text{In}_x\text{Ga}_{1-x}\text{As}/\text{GaAs}$  because it is the lowest energy level in the quantum well and is, therefore, highly responsible for radiative transition.

The splitting of the valence bands results in reduced effective hole mass and greatly improves the matching of the valence and conduction band density of states. Due to this characteristic, strained quantum wells utilize lower threshold carrier density to induce the population inversion condition. Hence, the performance of semiconductor lasers is improved by using a strained quantum well as an active layer.

Another important thing as discussed in several solid state textbooks e.g. ref. [6, 20] is that the light hole and heavy hole bands are responsible for optical polarization. Therefore, proper designs of strain layer can control the polarization of lasers.

## 2.5 Calculation results of quantized energy level in $\text{GaAs}/\text{Al}_x\text{Ga}_{1-x}\text{As}$ quantum wells

From the procedures outlined in section 2.2, quantized energy levels and thus the corresponding wavelength emitted from  $\text{GaAs}/\text{Al}_x\text{Ga}_{1-x}\text{As}$  quantum well structures are approximated. The details of the parameters used in the calculations and a fitting function are summarized in appendix A.

The temperatures used for these calculations are 0 K, 77 K, and 300 K with approximately equal to cryogenic closed circuit helium, liquid nitrogen, and room temperatures respectively. The Al contents are selected to be 0.1, 0.2, 0.3, and 0.4 and the well width is continuously varied from 5 – 150 Å. However, the strained effect is totally neglected in this structure because of the negligible lattice mismatch (smaller than 1%). Fig.2.8 – Fig.2.11 demonstrate the calculation results of energy levels in  $\text{GaAs}/\text{Al}_x\text{Ga}_{1-x}\text{As}$  quantum well,  $0.1 < x < .4$ .

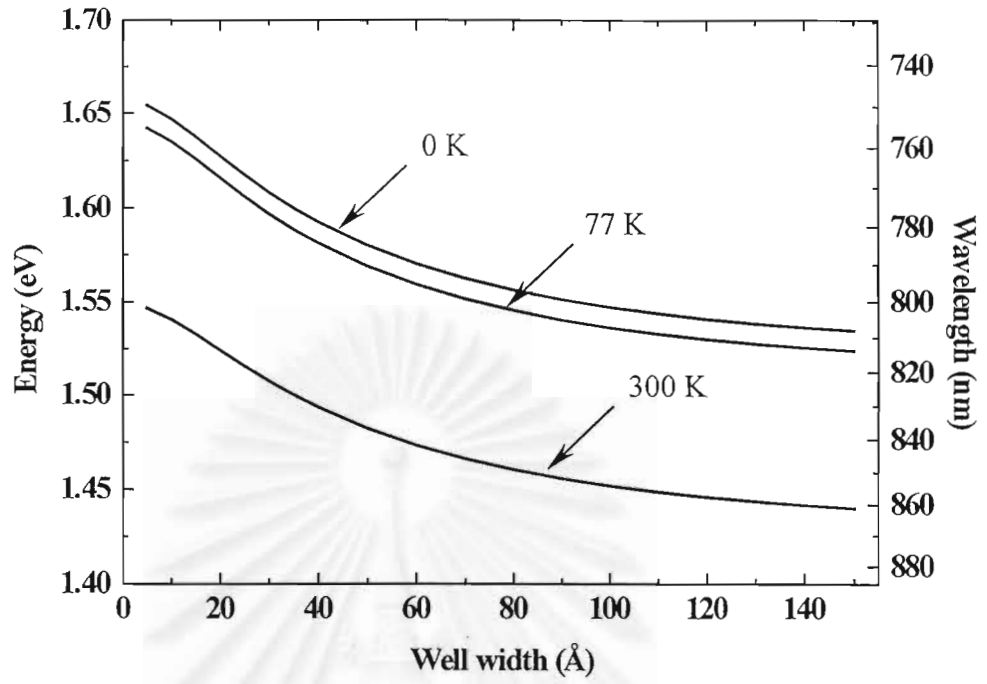


Fig. 2.8 Effective energy gap in the GaAs/Al<sub>0.1</sub>Ga<sub>0.9</sub>As quantum well

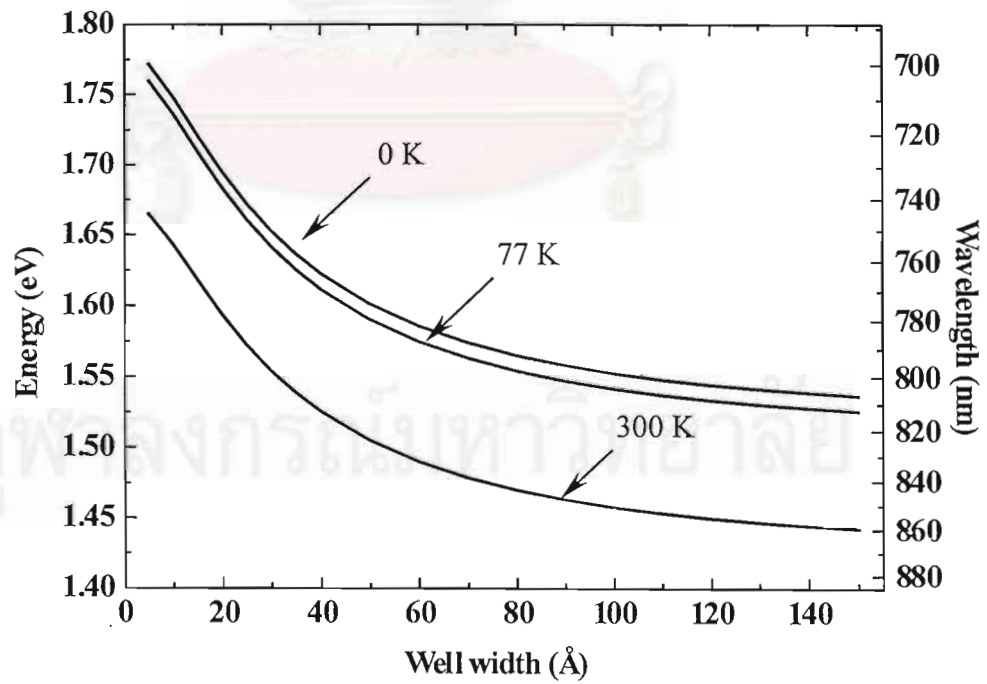


Fig. 2.9 Effective energy gap in the GaAs/Al<sub>0.2</sub>Ga<sub>0.8</sub>As quantum well

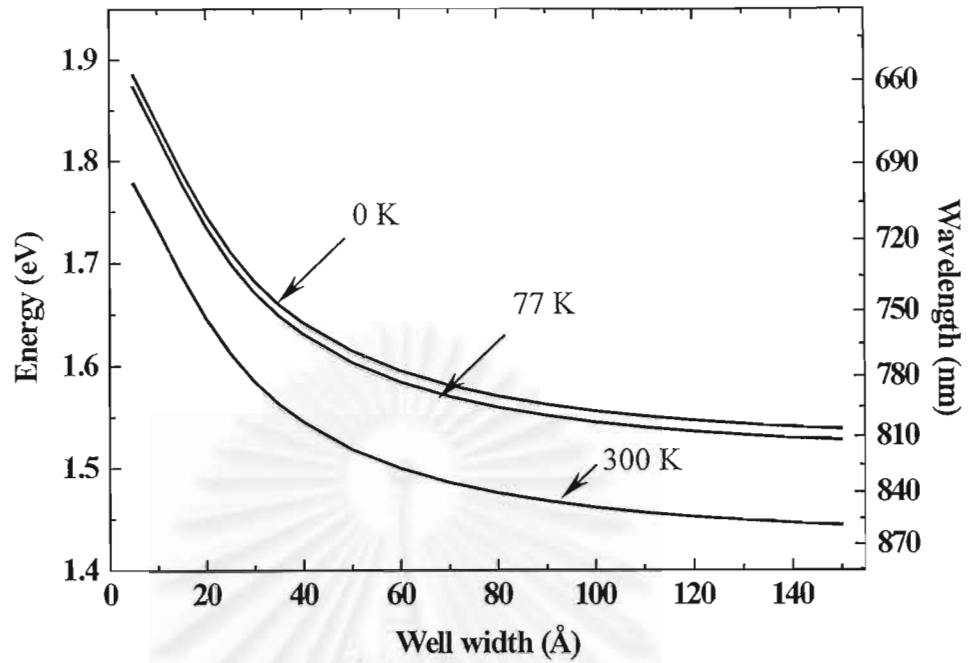


Fig. 2.10 Effective energy gap in the GaAs/Al<sub>0.3</sub>Ga<sub>0.7</sub>As quantum well

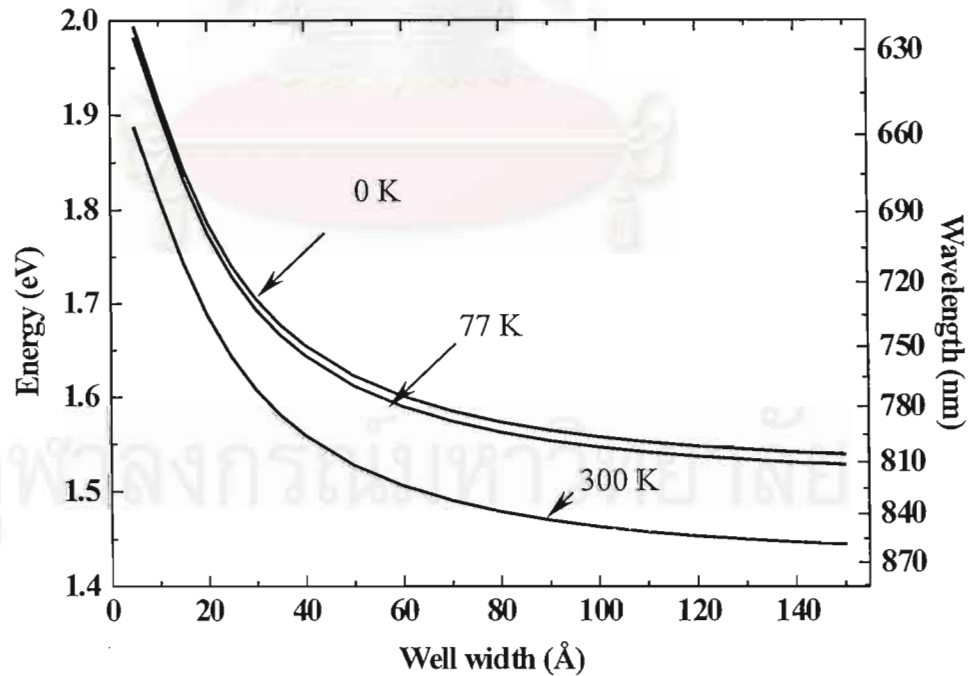


Fig. 2.11 Effective energy gap in the GaAs/Al<sub>0.4</sub>Ga<sub>0.6</sub>As quantum well

## 2.6 Calculation results of quantized energy level in $\text{In}_x\text{Ga}_{1-x}\text{As}/\text{GaAs}$ strained quantum well

The quantized energy levels of  $\text{In}_x\text{Ga}_{1-x}\text{As}/\text{GaAs}$  strained quantum well structure systems can also be calculated from the procedures given in section 2.2 but the effects of strain which was introduced in section 2.4 should be included. **Deformation potential theory** is applied in this calculation: the presence of strain shifts the energy levels in the strained layer at  $k_x = k_y = 0$ . The energy shifting parameters due to the strain, derived from this theory [17], are given in appendix A.

The specific temperatures used in the calculation are 0 K, 77 K, and 300 K as the previous section. The indium contents of 0.05, 0.10, 0.15, and 0.20 are selected; the well width is continuously varied from 5 – 150 Å. The calculation results of  $\text{InGaAs}/\text{GaAs}$  strained quantum well are shown in Fig. 2.12 – 2.15.

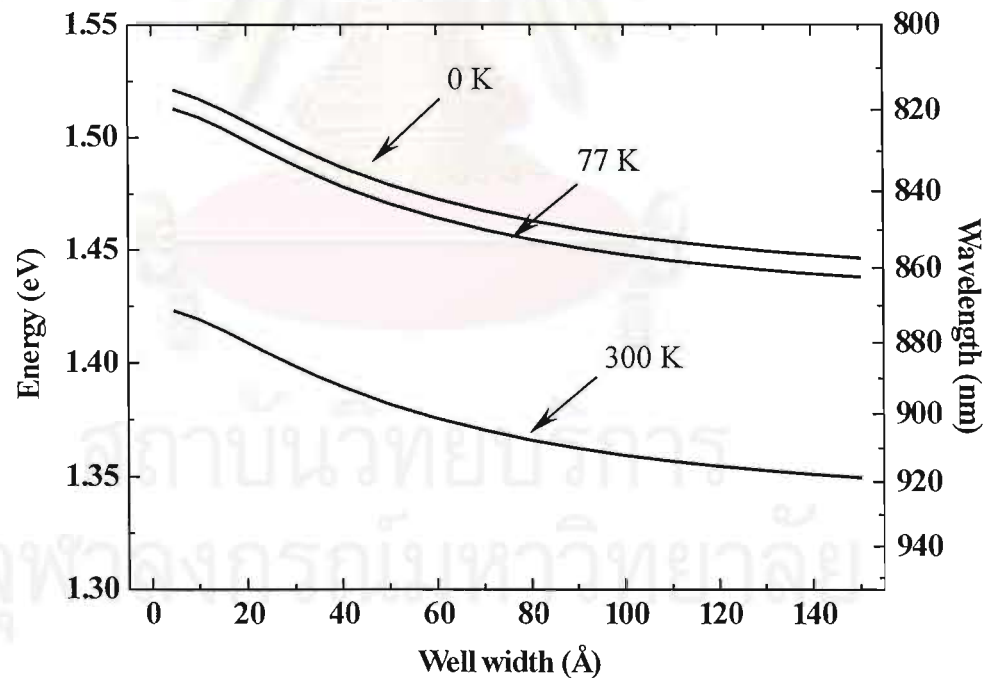


Fig. 2.12 Effective energy gap in the  $\text{In}_{0.05}\text{Ga}_{0.95}\text{As}/\text{GaAs}$  strained quantum well

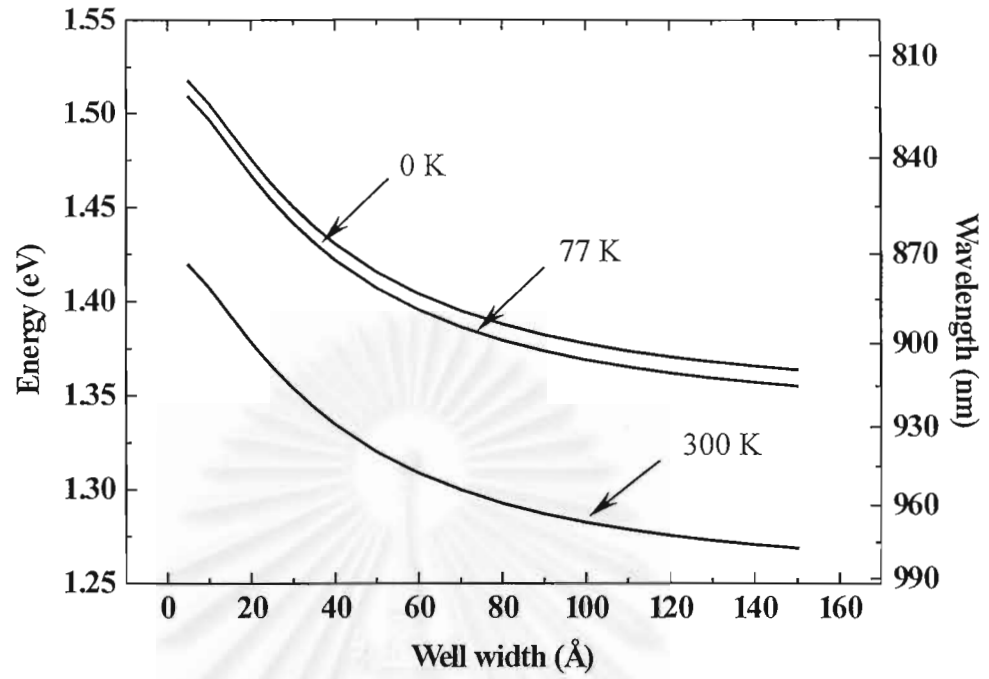


Fig. 2.13 Effective energy gap in the In<sub>0.10</sub>Ga<sub>0.90</sub>As/ GaAs strained quantum well

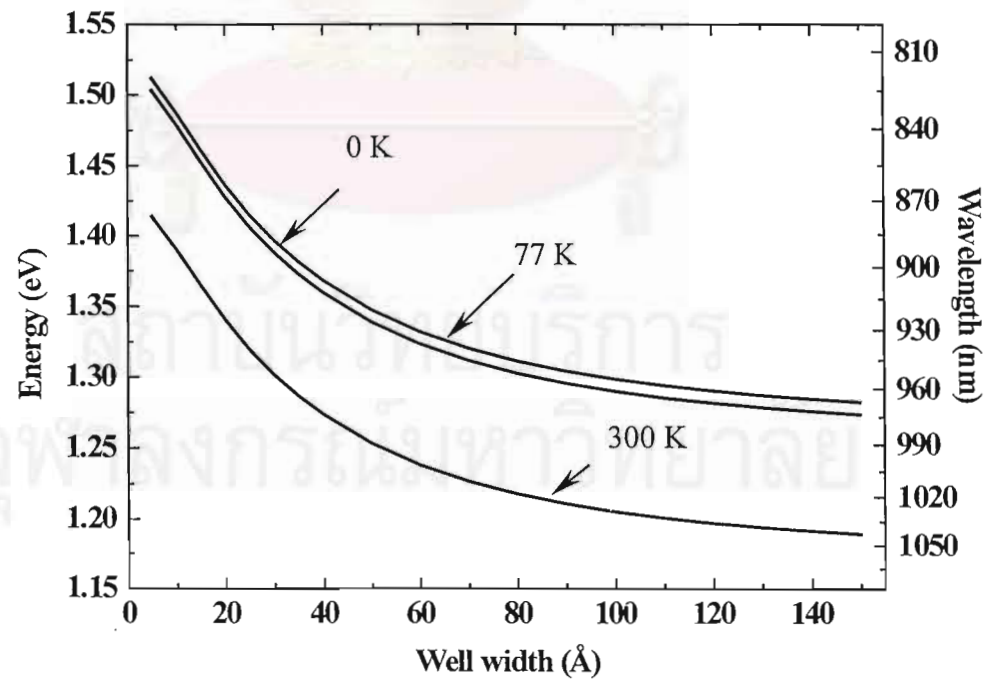


Fig. 2.14 Effective energy gap in the In<sub>0.15</sub>Ga<sub>0.85</sub>As/GaAs strained quantum well

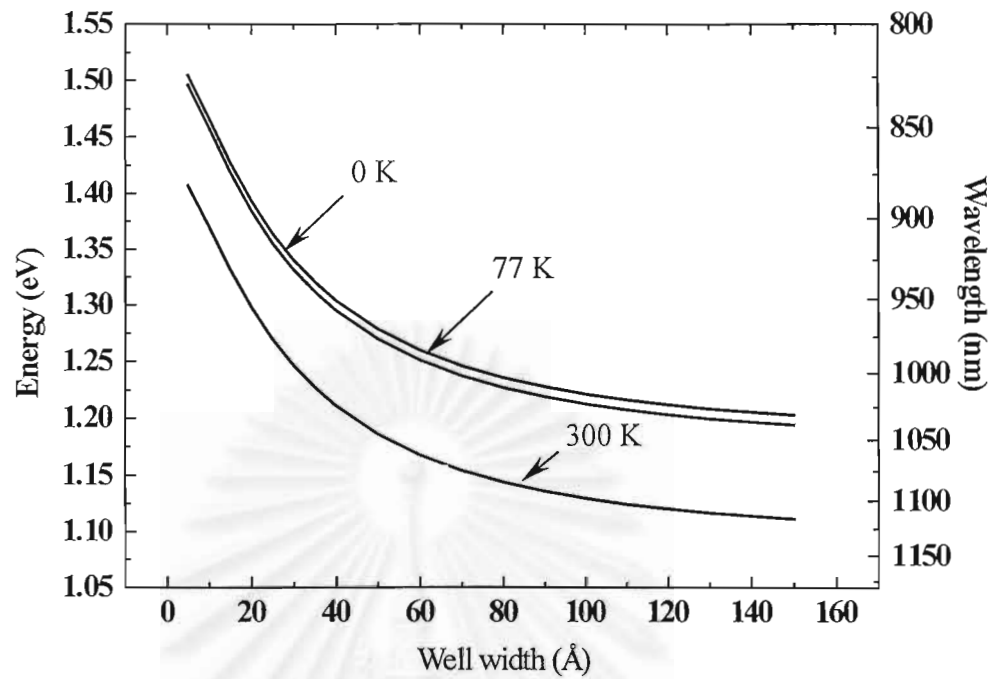


Fig. 2.15 Effective energy gap in the  $\text{In}_{0.20}\text{Ga}_{0.80}\text{As}/\text{GaAs}$  strained quantum well

### Conclusion

This chapter provides the approximated calculations of effective energy gap for  $\text{GaAs}/\text{Al}_x\text{Ga}_{1-x}\text{As}$  and  $\text{In}_x\text{Ga}_{1-x}\text{As}/\text{GaAs}$  system as a function of well width, well depth which is varied with Al and In contents, and temperature.



## CHAPTER 3

### Optical Gain in Quantum Well Structure

#### 3.1 Introduction

As discussed in Chapter 1, the efficiency of semiconductor lasers was improved from a homojunction structure to a heterojunction structure as a result of optical and electronic confinement properties. When the dimensionality of the active layer of the double heterojunction is reduced from 3D to 2D, its density of states change to be step-like which is a factor in reducing a threshold current.

In this chapter, the fundamental of optical gain which provides the understanding of laser actions in semiconductors is introduced. The details can be divided into 2 parts. The first part is related to a slab waveguide, a basic structure essential in the understanding of waveguide characteristics. The second part is about the optical gain in 3D and 2D systems, detailing the difference between quantum well and double heterostructure laser.

#### 3.2 Slab waveguide

A double-heterojunction is a structure with one semiconductor material sandwiched between two higher energy gap cladding layers. The refractive index discontinuity between the two materials gives the guiding property to this structure. In this section, a basic structure called **slab waveguide** (see Fig. 3.1) is discussed in detail [23-24].

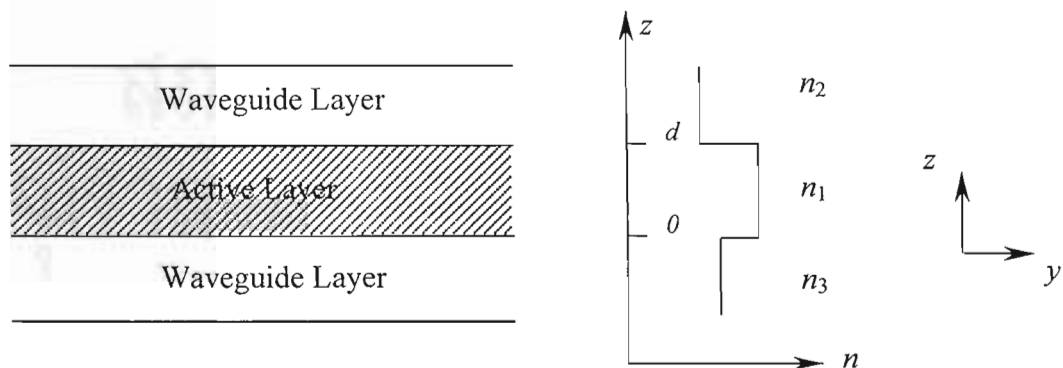


**Fig. 3.1** The one dimension slab waveguide [16-17]

Generally, guiding in the transverse direction is referred to as an **index guiding mechanism** which results from the refractive index discontinuities between the active and the cladding layers. The active layer has the highest refractive index ( $n_1 > n_2$  and  $n_1 > n_3$ ) and if  $n_2 \neq n_3$ , the structure is called **an asymmetric slab guide** whereas it is called a **symmetric slab guide** in case of  $n_2 = n_3$ . In this chapter, the solution only for a transverse electric field (the optical wave is polarized parallel to layers) is investigated.

First, we start with the time-independent wave equation assuming that the propagation is in the  $y$  direction:

$$\nabla^2 E_{xi}(y, z) + n_i^2 k_0^2 E_{xi}(y, z) = 0 \quad (3.1)$$

where the subscript  $i$  refers to the  $i^{\text{th}}$  layer,  $E_{xi}$  is the transverse electric field in each layer,  $n_i$  is the refractive index of the  $i^{\text{th}}$  layer,  $k_0$  is a propagation constant, the  $y$  and the  $z$  axes are the direction parallel and perpendicular to the heterointerface respectively (see Fig. (3.1) for notation). The solution to eq. (3.1) can be written in the form

$$E_{xi}(y, z) = E_i(z) \exp(-j\beta y) \quad (3.2)$$

where  $\beta$  is a constant to determine later.

From eqs. (3.2) and eq. (3.1), the electric field in each layer  $E_i(z)$  is given by

$$\frac{d^2 E_i}{dz^2} + [n_i^2 k_0^2 - \beta^2] E_i = 0 \quad (3.3)$$

or  $n_e$  is an effective refractive index and  $\beta^2 = k_0^2 n_e^2$ .

$$\frac{d^2 E_i}{dz^2} + [n_i^2 k_0^2 - k_0^2 n_e^2] E_i = 0 \quad (3.4)$$

The solutions for the optical wave confined in each layer are

$$\left. \begin{aligned} E_1(z) &= A \cos(\kappa z) + B \sin(\kappa z) & 0 \leq z \leq d \\ E_2(z) &= C e^{-\gamma z} + D e^{\gamma z} & z > d \\ E_3(z) &= F e^{-\gamma z} + G e^{\gamma z} & z < 0 \end{aligned} \right\} \quad (3.5)$$

where  $\gamma = k_0(n_2^2 - n_e^2)^{\frac{1}{2}}$  and  $\kappa = k_0(n_e^2 - n_1^2)^{\frac{1}{2}}$ , and  $A, B, C, D, F,$  and  $G$  are constants

The boundary conditions impose the following requirements: Firstly, the electric field at infinity is zero ( $E(\pm\infty) \rightarrow 0$ ). Secondly, the electric field ( $E_i$ ) and its gradient ( $\frac{dE_i}{dz}$ ) at the interfaces are continuous. From the first boundary condition, we obtain  $D = F = 0$ . From the second, we have

$$\tan(\kappa d) = \frac{2\kappa\gamma}{\kappa^2 - \gamma^2} \quad (3.6)$$

$n_e$  can be obtained from eq. (3.6) by graphically or numerically calculation.

The efficiency of waveguide is characterized by  $\Gamma$ , the **optical confinement factor** given by

$$\Gamma = \frac{\int_0^d |E(z)|^2 dz}{\int_{-\infty}^{+\infty} |E(z)|^2 dz} \quad (3.7)$$

which depends strongly on a waveguide structure and highly effects to the efficiency of semiconductor laser.

For a single quantum well structure, the confinement factor can be easily obtained by the method discussed above. However, for multiple quantum wells structure, the calculation is more complicated due to the presence of the active multi-layer. We can simplify the problem by approximating the refractive index of the multi-layer by [21].

$$n_{r\perp}^2 = \frac{n_w^2 n_b^2 (m_w d_w + m_b d_b)}{(n_w^2 m_b d_b + n_b^2 m_w d_w)}, \quad (3.8)$$

where  $n_{r\perp}$  is the effective transverse refractive index,  $n_w$  and  $n_b$  are the refractive index of the well and the barrier layer,  $d_w$ ,  $d_b$ ,  $m_w$  and  $m_b$  are the well thickness, the barrier thickness the well number, and the barrier number, respectively.

From eqs. (3.5)-(3.7), the confinement factor of GaAs/Al<sub>0.2</sub>Ga<sub>0.8</sub>As double heterostructure is obtained and shown in Fig. 3.2. The confinement factor of 50-150 Å active region of single quantum well is around 0-0.2. Thus, single quantum wells are not

suitable as a waveguide structure even though both the well (GaAs) and the barrier (AlGaAs) have suitable refractive indices.

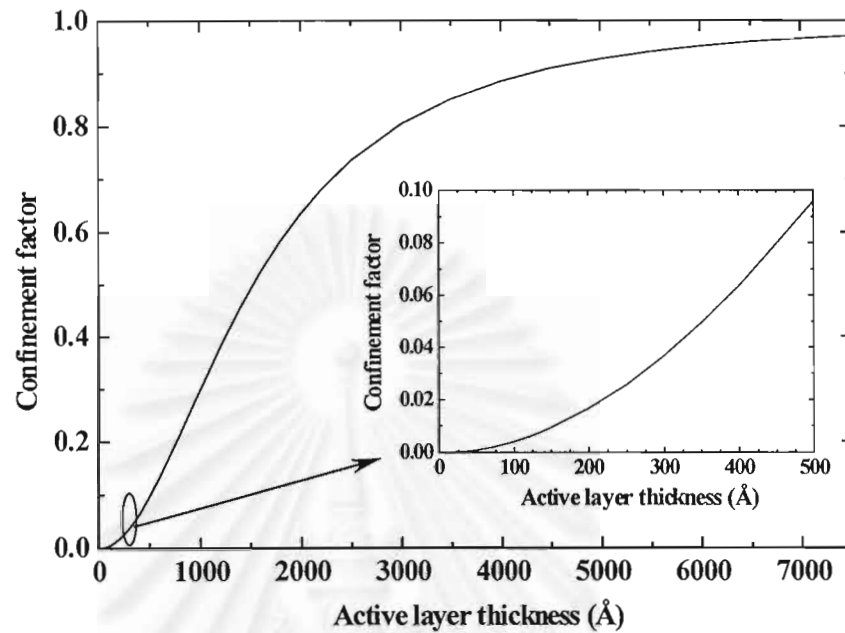


Fig. 3.2 The calculated confinement factor for the GaAs/Al<sub>0.2</sub>Ga<sub>0.8</sub>As double heterostructure. The inset shows the expand view in the quantum sized region.

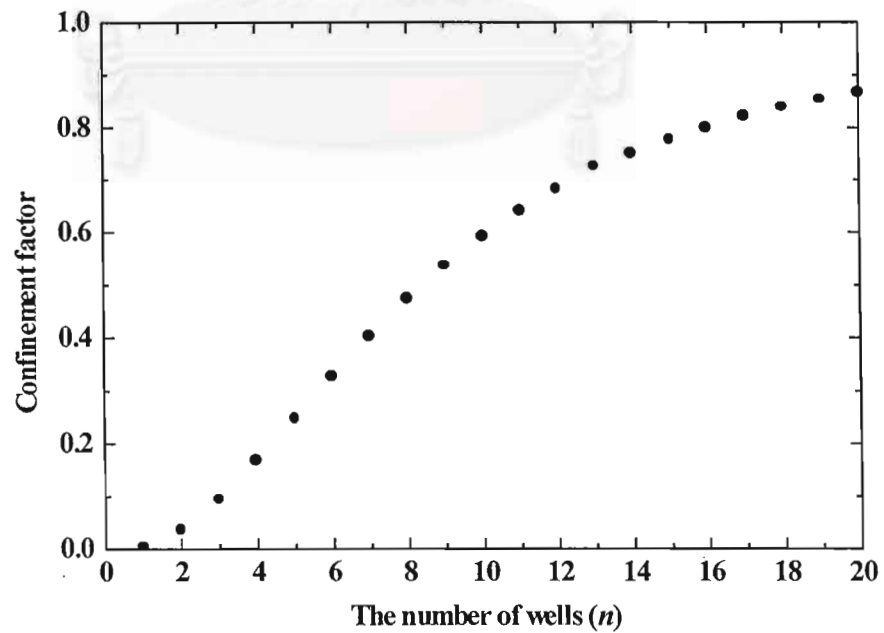


Fig. 3.3 The calculated confinement factor for the GaAs/Al<sub>0.2</sub>Ga<sub>0.8</sub>As multiple quantum wells with 100 Å well width and 300 Å barrier

To improve the guiding property, the multiple quantum well is referred. Guiding is seem to be improved with the increasing number of wells as seen in Fig. 3.3. The calculated confinement factor of multiple quantum wells is referred to eqs. (3.5)-(3.8) and the refractive indices used in the calculation are in ref. [25].

For InGaAs/GaAs systems, guiding is poor due to inappropriate refractive indices of the two materials. An alternative solution to improve the confining efficiency is to add a wave-guiding layer with suitable refractive index to the active layer.

### 3.3 Optical gain

The **optical gain** in semiconductor can be induced by external excitations such as photon excitation, electron excitation and current injection.

When carriers are injected to semiconductor, the electrons in valence band are excited to the conduction band. The probabilities of finding an electron or a hole at a particular energy level ( $E$ ) are

$$f_e(E) = \frac{1}{e^{\frac{E-F_n}{k_B T}} + 1} \quad \text{for electrons in the conduction band} \quad (3.9)$$

$$f_h(E) = \frac{1}{e^{\frac{F_p-E}{k_B T}} + 1} \quad \text{for holes in the valence band} \quad (3.10)$$

where  $F_n$  and  $F_p$  are the quasi-Fermi level for electrons and holes respectively,  $k_B$  is the Boltzmann's constant and  $T$  is the temperature. After sometimes, excited electrons in the conduction band recombine with holes in the valence band and release photon spontaneously, in case of a direct gap material.

Under high carrier injection, the conduction band (valence band) is partially filled with electrons (holes) which means that the probability of finding electrons in conduction band is larger than that in valence band. This is called a **population inversion condition**. From the definition of the population inversion and the carrier distribution in non equilibrium state from eq. (3.9)-eq. (3.10), we obtain

$$f_e(E) > 1 - f_h(E)$$

$$\frac{1}{e^{\frac{E\gamma_1 - F_n}{k_B T}} + 1} > 1 - \frac{1}{e^{\frac{F_p - E\gamma_2}{k_B T}} + 1}$$

$$F_n - F_p > E\gamma_1 - E\gamma_2 \quad (3.11)$$

where  $E_{\gamma_1}$  is the energy of the state  $\gamma_1$  in the conduction band and  $E_{\gamma_2}$  is the energy of the state  $\gamma_2$  in the valence band. As the minimum difference between these states is the band gap energy,  $E_g$ , we get

$$F_n - F_p > E_g \quad (3.12)$$

Under this condition, the electron-hole pairs could recombine and emit more photons than could be absorbed. The optical gain can be derived from

$$\text{gain} = \text{emission} - \text{absorption} \quad (3.13)$$

The gain is proportional to the probability of finding electrons in the conduction band and holes in the valence band as given by [17, 21-22, 26]:

$$g(E) \propto N_{cv}(E - E'_g)[f_e(E^e) - (1 - f_h(E^h))] \quad (3.14)$$

where  $E$  is the exciting photon energy,  $E'_g$  is the effective energy gap,  $N_{cv}$  is the reduced density of states. The superscript  $e$  and  $h$  are for electron and hole respectively.

For bulk materials:

$$E'_{g,3D} = E_c - E_v \quad (3.15)$$

$$N_{cv}^{3D} = \frac{1}{2\pi} \left[ \frac{2m_r^*}{\hbar^2} \right]^{\frac{3}{2}} (E - E'_g)^{\frac{1}{2}} \quad (3.16)$$

For quantum wells:

$$E'_{g,2D} = E_{e1} + E_g + E_{hh1} \quad (3.17)$$

$$N_{cv}^{2D} = \frac{m_r^*}{\pi\hbar^2} \quad (3.18)$$

The energies  $E^e$  and  $E^h$  are related to the photon energy as follows:



$$E^e = E_c + \frac{m_r^*}{m_e^*} (E - E'_g) \quad (3.19)$$

$$E^h = E_v - \frac{m_r^*}{m_h^*} (E - E'_g) \quad (3.20)$$

where  $\frac{1}{m_r^*} = \frac{1}{m_e^*} + \frac{1}{m_h^*}$  and  $m_r^*$ ,  $m_e^*$ , and  $m_h^*$  are the reduced effective mass, the electron effective mass and the hole effective mass respectively.

From eq. (3.14)-(3.20), the build up of gain in GaAs bulk  $(E - E'_g)^{-\frac{1}{2}}(f_e(E^e) + f_h(E^h) - 1)$  is plotted as a function of  $E$  at 77 K and 300 K in Figs. 3.4-3.5. The gain in bulk material increases from zero to the maximum value and then decreases to zero again at  $E = F_n - F_p$  which means that photons energy larger than  $F_n - F_p$  would be absorbed.

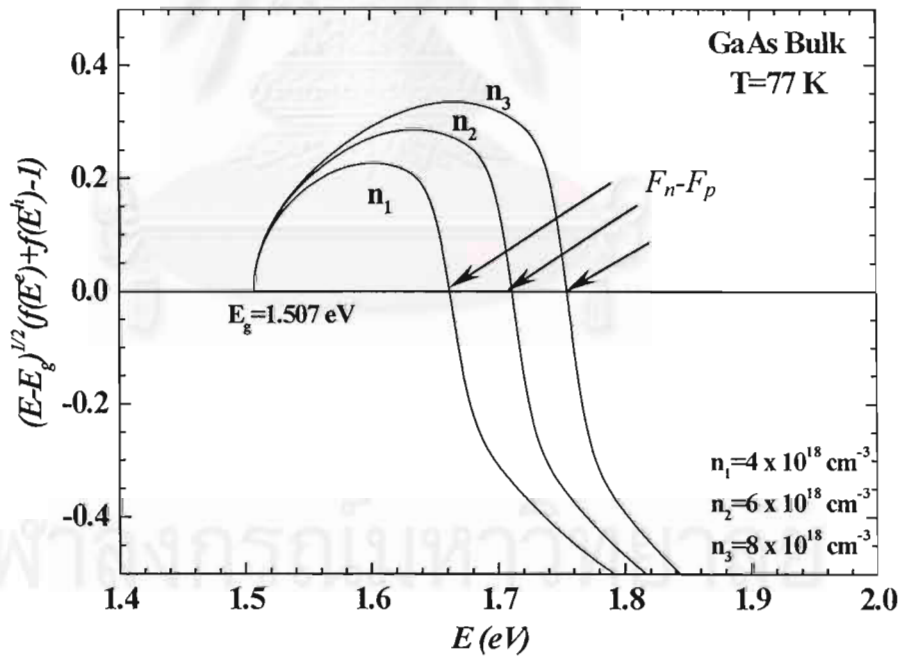


**Fig. 3.4** The function  $(E - E_g)^{-\frac{1}{2}}(f_e(E^e) + f_h(E^h) - 1)$  of bulk GaAs at 77 K for bulk carrier densities  $4 \times 10^{18}$ ,  $6 \times 10^{18}$ , and  $8 \times 10^{18} \text{ cm}^{-3}$



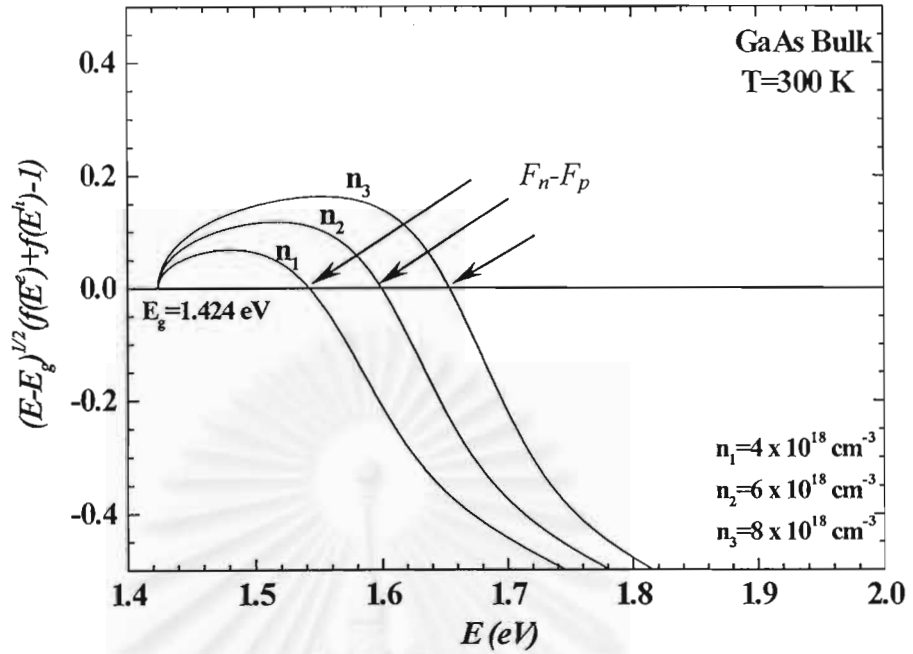


Fig. 3.5 The function  $(E - E_g)^{1/2} (f(E^e) + f(E^h) - 1)$  of bulk GaAs at 300 K for bulk carrier densities  $4 \times 10^{18}$ ,  $6 \times 10^{18}$ , and  $8 \times 10^{18} \text{ cm}^{-3}$

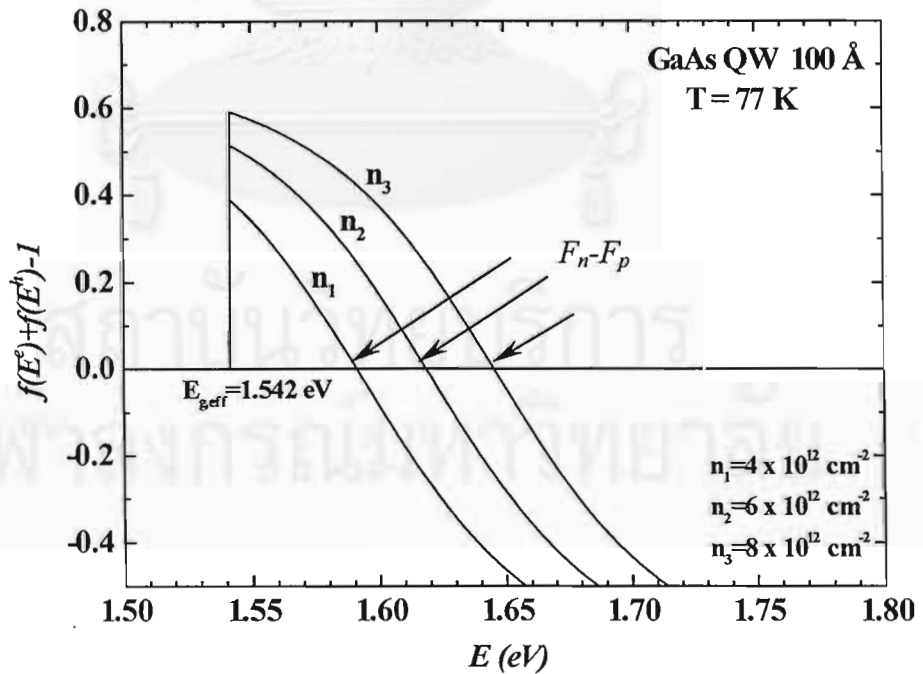
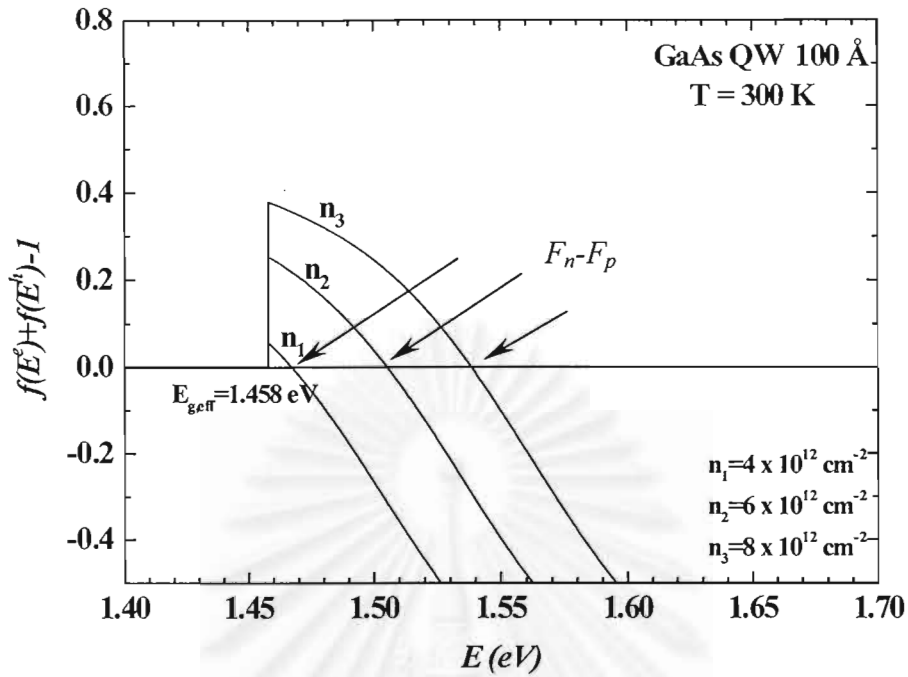


Fig. 3.6 The function  $f(E^e) + f(E^h) - 1$  of GaAs/Al<sub>0.2</sub>Ga<sub>0.8</sub>As quantum well with 100 Å well width at 300 K for sheet carrier densities  $4 \times 10^{12}$ ,  $6 \times 10^{12}$ , and  $8 \times 10^{12} \text{ cm}^{-2}$



**Fig. 3.7** The function  $f(E^e) + f(E^h) - 1$  of GaAs/Al<sub>0.2</sub>Ga<sub>0.8</sub>As quantum well with 100 Å well width at 300 K for sheet carrier densities  $4 \times 10^{12}$ ,  $6 \times 10^{12}$ , and  $8 \times 10^{12}$  cm<sup>-2</sup>

Figures 3.6 and 3.7 show the plot  $f_e(E^e) + f_h(E^h) - 1$  as a function of  $E$  of GaAs/Al<sub>0.2</sub>Ga<sub>0.8</sub>As quantum well with 100 Å well width at 77 K and 300 K respectively. Since the density of states of quantum wells is constant, there are a group of electrons and a group of holes at nearly the same energy in the conduction and the valence band available to recombine. This results in an efficient carrier injection into the quantum well because the added carriers contribute to the peak gain. On the other hand, in bulk materials, the maximum gain stays away from the bandedge which makes all carriers at an energy below that of  $g_{\max}$  useless.

In a strained quantum well, as discussed in Chapter 2, the lower effective hole mass reduces the carrier density needed for population inversion. Figures 3.8 and 3.9 show the plots of  $f(E^e) + f(E^h) - 1$  as a function of  $E$  of In<sub>0.2</sub>Ga<sub>0.8</sub>As/GaAs quantum well. It is clear that the gain region of this structure is larger than that of GaAs/Al<sub>0.2</sub>Ga<sub>0.8</sub>As quantum well with the same carrier densities.

From Figs. 3.4-3.9, we can clearly understand that the carrier injection efficiency of quantum well is higher than that of bulk and it can be further improved, if strains are introduced into the systems.

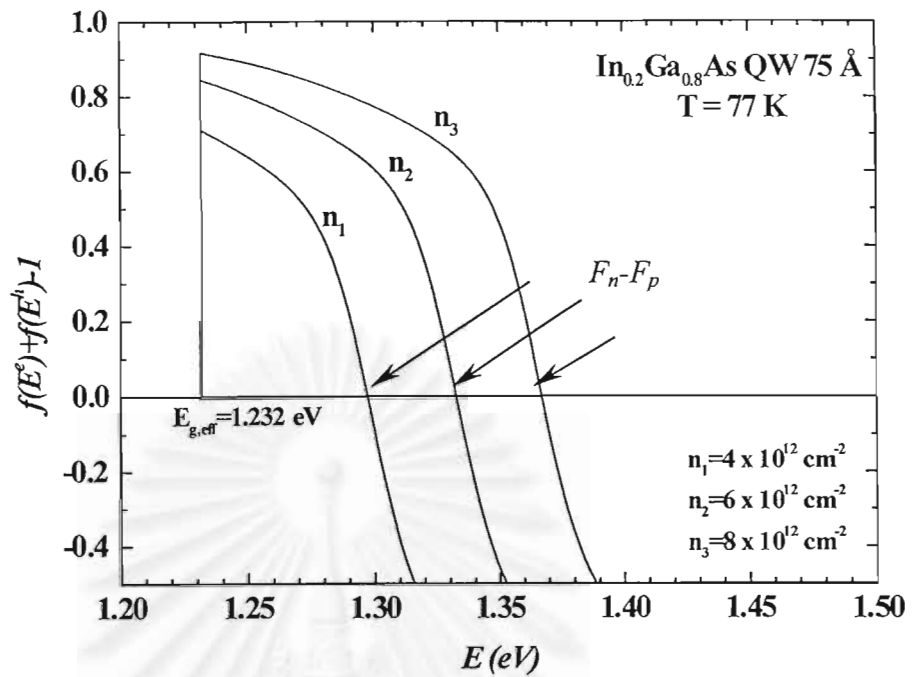


**Fig. 3.8** The function  $f(E^e) + f(E^h) - 1$  of  $\text{In}_{0.2}\text{Ga}_{0.8}\text{As}/\text{GaAs}$  quantum well with  $75 \text{ \AA}$  well width at  $77 \text{ K}$  for sheet carrier densities  $4 \times 10^{12}$ ,  $6 \times 10^{12}$ , and  $8 \times 10^{12} \text{ cm}^{-2}$

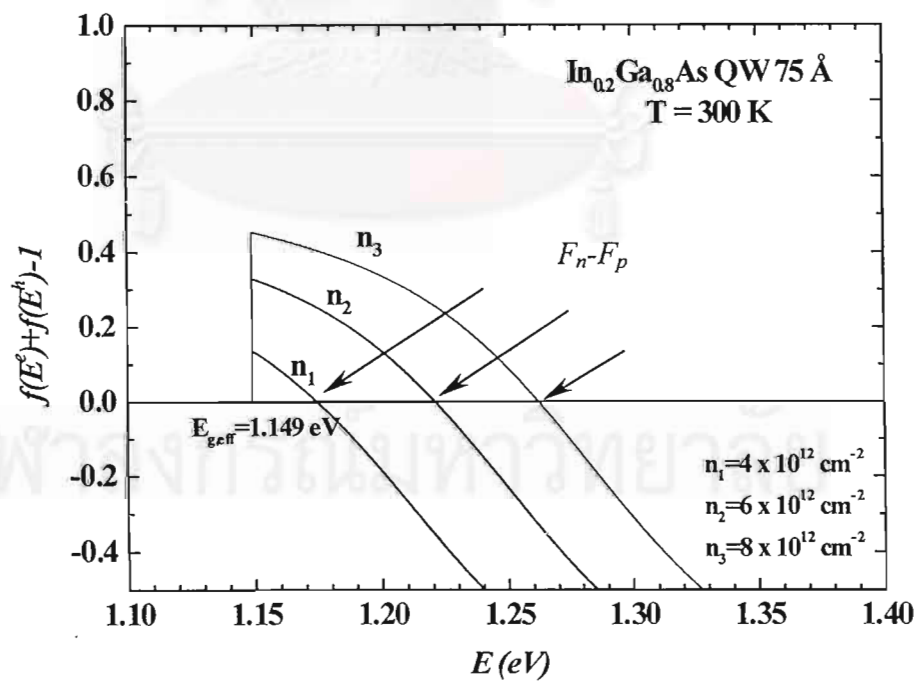


**Fig. 3.9** The function  $f(E^e) + f(E^h) - 1$  of  $\text{In}_{0.2}\text{Ga}_{0.8}\text{As}/\text{GaAs}$  quantum well with  $75 \text{ \AA}$  well width at  $300 \text{ K}$  for sheet carrier densities  $4 \times 10^{12}$ ,  $6 \times 10^{12}$ , and  $8 \times 10^{12} \text{ cm}^{-2}$

The relation between  $g_{\max}$  and carrier densities [27] is as follows:

$$g_{\max} \propto f_{e,c}(n) - f_{e,v}(n) \quad (3.21)$$

where  $f_{e,c}(n)$  and  $f_{e,v}(n)$  are the electron distribution at the conduction and the valence band, respectively. Charge neutrality is assumed in eq. (3.21). Therefore, the Fermi function can be related to the electron and hole densities by a simple approximation (only  $g_{\max}$  of quantum well is discussed):

For the number of electrons in the conduction band:

$$n = \int_{E_c}^{\infty} N_{c,2D}(E) f_{e,c}(E) dE \quad (3.22)$$

For the number of holes in the valence band:

$$p = \int_{-\infty}^{E_v} N_{v,2D}(E) f_{h,v}(E) dE \quad (3.23)$$

where  $n$  ( $p$ ) is the electron (hole) densities,  $f_{h,v}(E)$  is the hole distribution in the valence

band,  $N_{c,2D}(E) = \frac{m_e^*}{\pi \hbar^2} \left( \frac{1}{L_z} \right)$  is the conduction band density of states, and

$N_{v,2D}(E) = \frac{m_h^*}{\pi \hbar^2} \left( \frac{1}{L_z} \right)$  is the valence band density of states. Thus, we obtain

$$f_{e,c}(E) = 1 - e^{-\frac{n}{N_{c,2D}}} \quad (3.24)$$

$$f_{e,v} = 1 - f_{h,v}(E) = 1 - (1 - e^{-\frac{p}{N_{v,2D}}}) = e^{-\frac{p}{N_{v,2D}}} \quad (3.25)$$

From eqs. (3.21) and eq. (3.24) – (3.25), the increases in the maximum gain with injected carrier densities are plotted in Figs. 3.10 and 3.11 for GaAs/Al<sub>0.2</sub>Ga<sub>0.8</sub>As single quantum well and In<sub>0.2</sub>Ga<sub>0.8</sub>As/GaAs strained single quantum well. From these figures, the **transparency carrier density**, the carrier density required at which  $g_{\max} = 0$ , can be obtained. The transparency carrier density in In<sub>0.2</sub>Ga<sub>0.8</sub>As/GaAs strained quantum well is lower than that of GaAs/Al<sub>0.2</sub>Ga<sub>0.8</sub>As unstrained case, which implies that the threshold current density of strained quantum well lasers would be smaller.

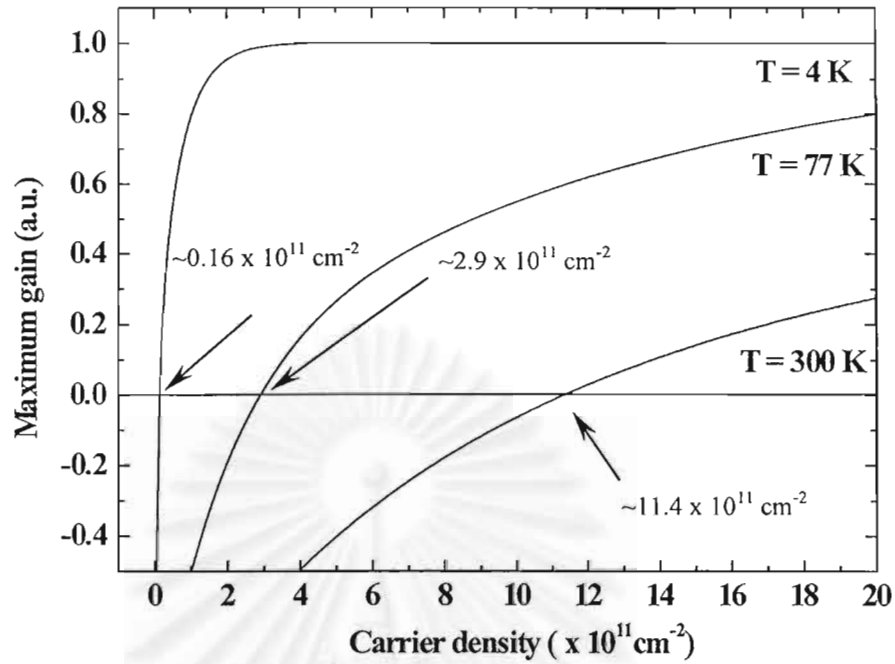


**Fig. 3.10** The maximum gain shape,  $f_{e,c}(n) - f_{e,v}(n)$ , of GaAs/Al<sub>0.2</sub>Ga<sub>0.8</sub>As single quantum well with 100 Å well width as a function of carrier density ( $n$ ).

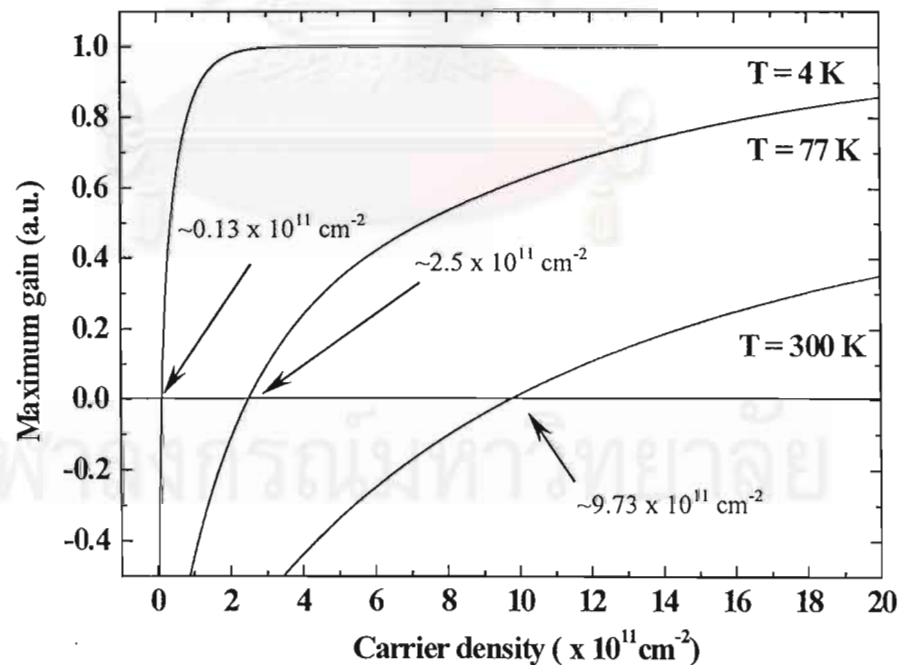


**Fig. 3.11** The maximum gain shape,  $f_{e,c}(n) - f_{e,v}(n)$ , of In<sub>0.2</sub>Ga<sub>0.8</sub>As/GaAs strained single quantum well with 75 Å well width as a function of carrier density ( $n$ ).

### The modal gain

The threshold current density of a semiconductor laser depends on the optical gain of the material and the laser structure. The **modal gain** ( $G$ ), which includes the confinement factor and the material gain, eq. (3.26), is a parameter used in the evaluation of the efficiency of lasers.

$$G = \Gamma \cdot g_{\max} \quad (3.26)$$

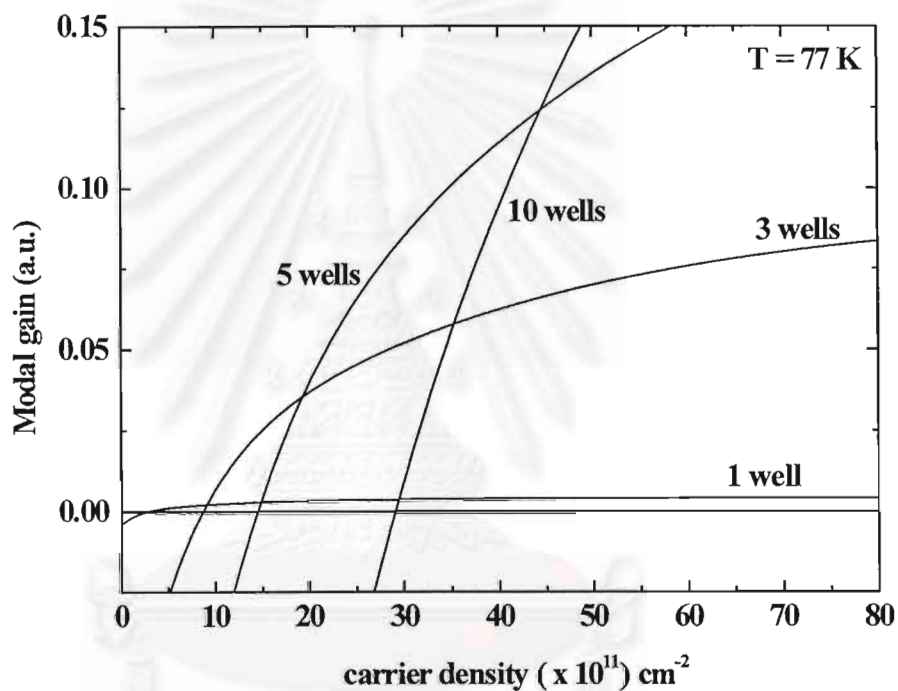


**Fig. 3.10** The modal gain shape,  $\Gamma \cdot (f_{e,c}(n) - f_{e,v}(n))$ , of GaAs/Al<sub>0.2</sub>Ga<sub>0.8</sub>As quantum wells with 100 Å well width as a function of carrier density ( $n$ )

The modal gains of GaAs/Al<sub>0.2</sub>Ga<sub>0.8</sub>As quantum well with 1, 3, 5, and 10 wells are plotted as a function of carrier density in Fig. 3.12. Due to larger confinement factor, the higher the number of quantum wells, the higher the modal gains. However, the large density of states of multiple quantum well is responsible for the high transparency carrier density. As a consequence, we have to optimize between the gain needed to overcome the loss and the transparency carrier density, which is the minimum requirement for inducing gain.



## CHAPTER 4

### Fabrication and Measurement Technique

In this chapter, the details of fabrication process and measurement setup are presented. The fabrication processes are divided into 4 sections i.e. substrate preparation, flux calibration, growth, and optical cavity fabrication. The second part, the measurement setup consists of 2 sections i.e. photoluminescence and the optically pumped measurement technique.

#### 4.1 Fabrication process

##### 4.1.1 Substrate preparation

The growth of III-V compound semiconductors are mostly performed on (100) oriented GaAs substrates by MBE. Generally, the (100) GaAs wafer (before loading into MBE system) is chemically cleaned [3, 28-30]. The wafer is successively boiled in trichloroethylene, acetone and then rinsed with de-ionized water. After being boiled in hydrochloric acid, the substrate is etched in the solution  $\text{H}_2\text{SO}_4: \text{H}_2\text{O}_2: \text{H}_2\text{O}$  3:1:1 [28]. Finally, the substrate is rinsed with de-ionized water and blown dry with nitrogen gas before mounting on molybdenum block with or without indium glue. The molybdenum block with GaAs substrate is then loaded into the preparation chamber and preheated at the temperature within the congruent evaporation region of GaAs. The preheating process in vacuum removes  $\text{H}_2\text{O}$ ,  $\text{O}_2$ , C and other surface contaminants [28-30].

In this experiment, the (100) oriented *n*-type GaAs substrates are epi-ready type and kept in a dust-free condition so the chemical cleaning process is, thus, not necessary. After mounting on the molybdenum block with indium glue, the GaAs substrate is preheated at 450 °C for 2 hours in the preparation chamber.

##### 4.1.2 Flux calibration

The major parameter used for controlling the growth rate is the constituent element flux pressure of the fabricated layer. Reference [28] determines that the growth rate of 1.3  $\mu\text{m/hr}$  for a GaAs layer is obtained with a gallium flux which gives a partial pressure about  $7 \times 10^{-7}$  torr. However, to ensure that the growth rate of the fabricated layer is as required,

the structure shown in Fig. 4.1 was fabricated and then selectively etched to measure the growth rate.

GaAs 2 $\mu\text{m}$
$\text{Al}_{0.5}\text{Ga}_{0.5}\text{As}$ 0.5 $\mu\text{m}$
GaAs buffer 0.25 $\mu\text{m}$
(100) n-type GaAs substrate

**Fig. 4.1** The structure designed to calibrate growth rate with the gallium flux

The flux pressure for the desired thickness and growth rate of Fig 4.1 was calculated from [19] as shown in Table 4.1.

**Table 4.1** The flux pressure with corresponding calculated growth rate

Element	Flux pressure	Growth rate		Calculated thickness	Measured thickness
			(calculation from ref [28])		
Ga	$4 \times 10^{-7}$ torr	GaAs	0.75 $\mu\text{m/hr}$	2 $\mu\text{m}$	1.6 $\mu\text{m}$
Al	$2.2 \times 10^{-7}$ torr	$\text{Al}_{0.5}\text{Ga}_{0.5}\text{As}$	1.5 $\mu\text{m/hr}$	1 $\mu\text{m}$	1 $\mu\text{m}$

\* As-riched conditions

After the growth,  $\text{Al}_{0.5}\text{Ga}_{0.5}\text{As}$  layer was selectively etched by KI: I<sub>2</sub>: H<sub>2</sub>O (12 g: 3 g: 10 ml) for 5 –10 second. The color of the etched layer would be different from the other layers. The GaAs thickness could then be measured by the optical microscope. The calibrated growth rate for GaAs layer is **1.05  $\mu\text{m/hr}$  with the gallium flux pressure is  $7 \times 10^{-7}$  torr.** This is the condition adapted throughout.

#### 4.1.3 Growth process

- ***In-situ* measurement**

The *in-situ* thickness monitoring in the growth chamber is called **RHEED** (Reflection High Energy Electron Diffraction) monitoring. This method assumes that the penetration of the electron beam restricted to the outermost layer of the crystal surface. Thus, only the first layer contributes to the diffraction pattern [3, 29-30]. The pattern contains the information from the topmost layer of the deposited material which can be related to the surface crystallography, proper growth condition and growth kinetics in the

MBE system. Atomic configuration at the outermost surface is different from bulk crystal structure for the lowest energy configuration and the most stable structure of (100) GaAs is the  $(2 \times 4)$  structure.

To observe the RHEED pattern, the substrate is heated up to a proper growth temperature in an As-stabilized atmosphere (to prevent congruent element evaporated from the substrate surface). At low temperatures, RHEED pattern is spotty as a result of the oxide on the surface. When the temperature increases to  $550^{\circ}\text{C}$ - $580^{\circ}\text{C}$  [3, 28-29, 31-33], the surface oxide is thermally desorbed from the substrate surface and the spotty pattern evolves in to a streaky pattern, indicative of an atomically clean surface ready for further growth. Examples of RHEED patterns and the corresponding surface morphology are shown in Fig. 4.2.

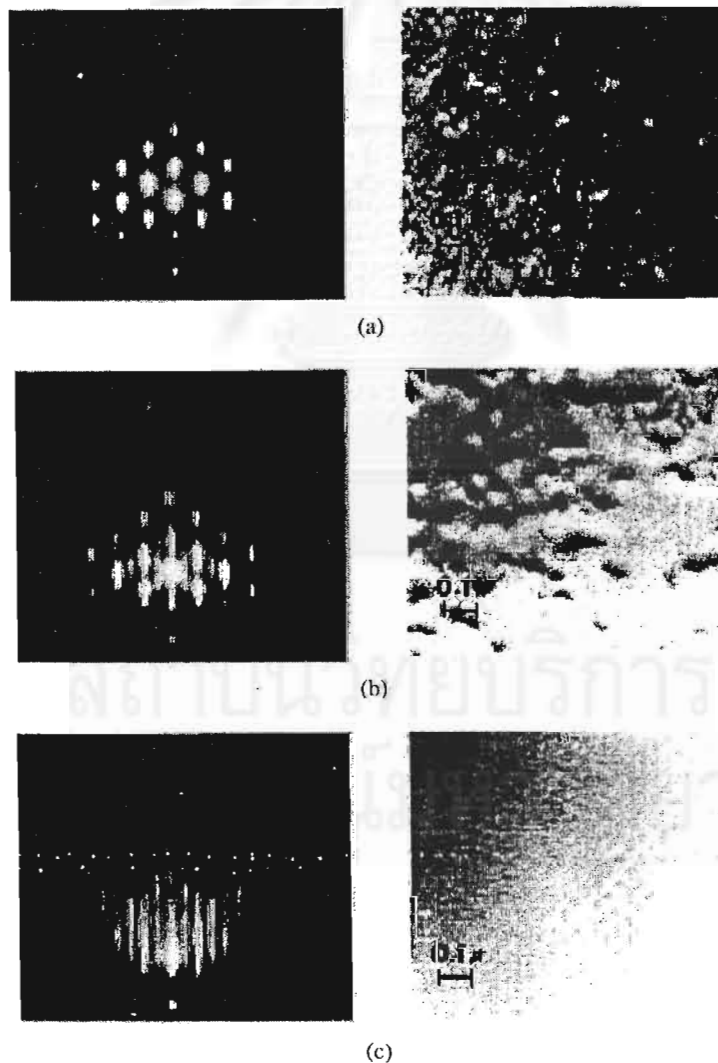


**Fig. 4.2** Examples of RHEED patterns (left) of GaAs substrate and surface morphology (right) [31]

- **Growth technique**

After the preheat treatments in the preparation chamber, the substrate is transferred to the growth chamber. The substrate temperature is heated under an As-stabilized condition, to prevent As desorbed from GaAs surface during growth [29, 31], until a streaky RHEED pattern is observed. The substrate is then held at that temperature for a few minutes after which a 1  $\mu\text{m}$  GaAs buffer layer is grown to ensure that the surface is smooth and clean. The substrate is then adjusted to the desired temperature.

A major factor affecting the epitaxial layer quality is the growth temperature. A common problem encountered in the substrate temperature control is the accuracy of the true temperature measurement during growth. The conventional technique using a contact thermocouple at the manipulator (as adopted in the MBE Riber32P system at Chulalongkorn University) gives varying results in different systems. Thus, the growth temperatures reported from many groups are difficult to compare. One useful way to evaluate the growth temperature is to approximate the temperature which results in the streaky RHEED pattern ( $T_{\text{RHEED}}$ ) about 580  $^{\circ}\text{C}$  (so this temperature is used for calibrating in our fabrication.).

The quantum well structures considered can be classified into 2 systems: the **lattice matched** (GaAs/ $\text{Al}_x\text{Ga}_{1-x}\text{As}$ ) and **lattice mismatched** ( $\text{In}_x\text{Ga}_{1-x}\text{As}/\text{GaAs}$ ) systems.  $\text{In}_x\text{Ga}_{1-x}\text{As}$  layers should be grown at a lower temperature than GaAs (around 500-550  $^{\circ}\text{C}$  [3, 31, 34 -37]). This comes from the fact that In atoms desorb from InGaAs surface considerably faster than Ga atoms. (In sticking coefficient is lower than that of Ga). Higher growth temperature causes more In desorption and then causes the undesired In content of the growth layer.

$\text{Al}_x\text{Ga}_{1-x}\text{As}$  layers, on the other hand, should be grown at a higher temperature than GaAs and  $\text{In}_x\text{Ga}_{1-x}\text{As}$  layers [3, 31]. Although the higher temperature results in the higher quality of the epitaxial layer, the upper limit should be restricted by the As arrival rate which prevents the element evaporating from the GaAs surface [31].

- **Growth structure**

The structures grown for the optically pumped experiment are shown in Fig. 4.3 – Fig. 4.4. The growth conditions for these samples are stated below:

### GaAs/Al<sub>x</sub>Ga<sub>1-x</sub>As system

#### GaAs/Al<sub>0.2</sub>Ga<sub>0.8</sub>As SQW (Fig. 4.3(a))

After depositing the 0.6 μm GaAs buffer layer on *n*-type GaAs (100) oriented substrate, a SQW consisting of a 1.25 μm Al<sub>0.2</sub>Ga<sub>0.8</sub>As barrier, 100 Å of GaAs well, and 0.25 μm upper barrier is grown. The growth temperature is 630 °C.

#### GaAs/Al<sub>0.2</sub>Ga<sub>0.8</sub>As 10 MQW (Fig. 4.3(b))

The 0.5 μm GaAs buffer was deposited at 630°C and then immediately followed by the deposition of 300 Å of Al<sub>0.2</sub>Ga<sub>0.8</sub>As barrier and 100 Å of GaAs well, repeated 10 times. The topmost layer is a 100 Å GaAs cap layer.

#### GaAs/Al<sub>0.2</sub>Ga<sub>0.8</sub>As 5 MQW with waveguide structure\* (Fig. 4.3(c))

The 0.1 μm GaAs buffer and 1 μm Al<sub>0.4</sub>Ga<sub>0.6</sub>As was deposited at 730°C followed by the 400 Å of Al<sub>0.2</sub>Ga<sub>0.8</sub>As barrier. Then, the deposition of 100 Å Al<sub>0.2</sub>Ga<sub>0.8</sub>As barrier and 75 Å GaAs well is repeated for 5 times. Finally, 400 Å of Al<sub>0.2</sub>Ga<sub>0.8</sub>As, 1000 Å of Al<sub>0.4</sub>Ga<sub>0.6</sub>As and 100 Å GaAs cap layer were grown.

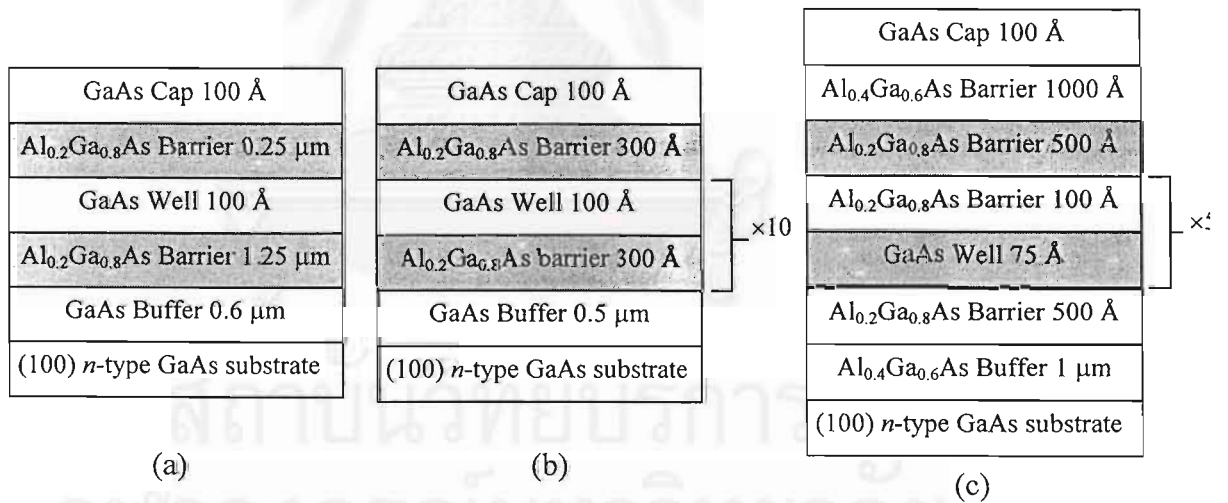


**Fig.4.3** GaAs/Al<sub>0.2</sub>Ga<sub>0.8</sub>As quantum well samples represented for lattice matched system (a) GaAs/Al<sub>0.2</sub>Ga<sub>0.8</sub>As SQW, (b) GaAs/Al<sub>0.2</sub>Ga<sub>0.8</sub>As 10 MQW, and (c) GaAs/Al<sub>0.2</sub>Ga<sub>0.8</sub>As 5 MQW with waveguide structure

\* Fabricated by Dr. Karl Eberl, MBE Group in Max-Planck Institute, Stuttgart, Germany.



### $\text{In}_x\text{Ga}_{1-x}\text{As}/\text{GaAs}$ systems

The growth conditions for InGaAs systems are quite different from the previous AlGaAs systems. In each sample in this experiment, the GaAs buffer layer is grown at  $T_{\text{RHEED}}$  and then the temperature is decreased below  $T_{\text{RHEED}}$ ; InGaAs layer is then grown.

#### $\text{In}_{0.2}\text{Ga}_{0.8}\text{As}/\text{GaAs}$ SQW (Fig.4.4 (a))

The 0.5  $\mu\text{m}$  GaAs buffer and the 0.125  $\mu\text{m}$  GaAs barrier are deposited at 595  $^\circ\text{C}$  on the substrate. Then 75  $\text{\AA}$  of  $\text{In}_{0.2}\text{Ga}_{0.8}\text{As}$  well followed by 0.125  $\mu\text{m}$  of GaAs barrier are grown at 545  $^\circ\text{C}$ .

#### $\text{In}_{0.2}\text{Ga}_{0.8}\text{As}/\text{GaAs}$ 3 MQW (Fig.4.4 (b))

The 0.5  $\mu\text{m}$  GaAs buffer and the 0.125  $\mu\text{m}$  GaAs barrier are deposited at 570  $^\circ\text{C}$  on the substrate. After that, 3 sets of  $\text{In}_{0.2}\text{Ga}_{0.8}\text{As}$  well and 400  $\text{\AA}$  of GaAs barrier are grown at 530  $^\circ\text{C}$ .

#### $\text{In}_{0.2}\text{Ga}_{0.8}\text{As}/\text{GaAs}$ 5 MQW (Fig.4.4 (c))

The 0.5  $\mu\text{m}$  GaAs buffer and the 0.125  $\mu\text{m}$  GaAs barrier are deposited at 570  $^\circ\text{C}$  on the substrate. After that, 5 sets of  $\text{In}_{0.2}\text{Ga}_{0.8}\text{As}$  well and 400  $\text{\AA}$  of GaAs barrier are grown at 530  $^\circ\text{C}$ .

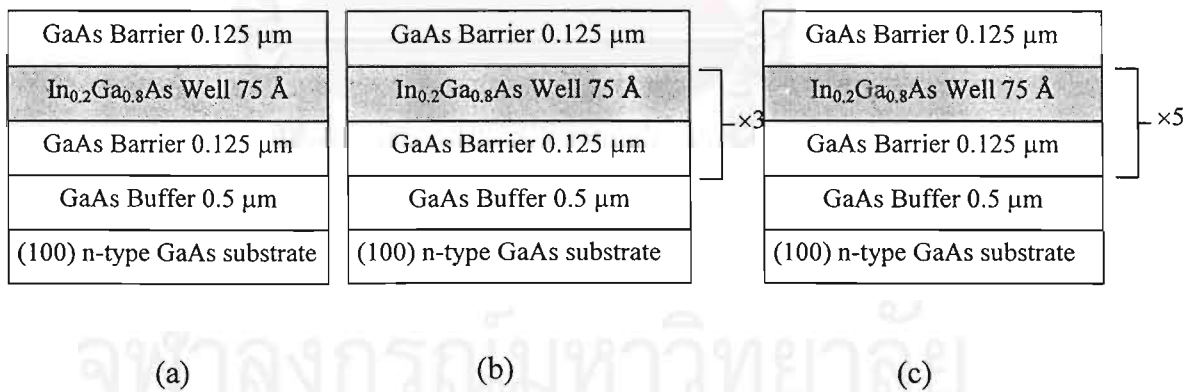


**Fig. 4.4**  $\text{In}_{0.2}\text{Ga}_{0.8}\text{As}/\text{GaAs}$  quantum well samples represented for lattice mismatched system (a)  $\text{In}_{0.2}\text{Ga}_{0.8}\text{As}/\text{GaAs}$  SQW, (b)  $\text{In}_{0.2}\text{Ga}_{0.8}\text{As}/\text{GaAs}$  3 MQW, and (c)  $\text{In}_{0.2}\text{Ga}_{0.8}\text{As}/\text{GaAs}$  5 MQW



#### 4.1.4 Optical cavity fabrication

After MBE process, the optical cavity was fabricated into qualified sample which were passed the photoluminescence measurement as described in section 4.2. To produce the high quality cleaved facets, operate as mirrors of the optical cavity, the substrate was thinned by lapping process. The process flow is shown in Fig. 4.5.

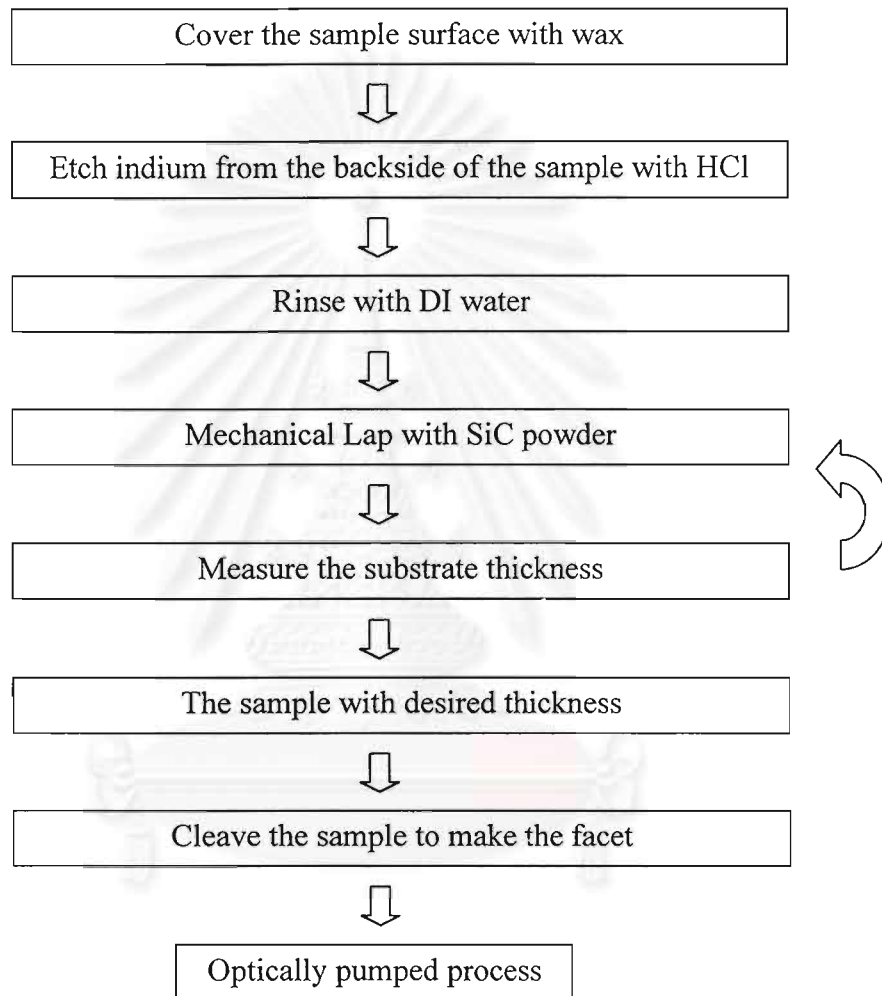


**Fig. 4.5** Optical cavity fabrication process

At first, the sample is mounted on the molybdenum block with indium glue so the backside of the sample should be etched by hydrochloric acid (HCl) before the mechanical lapping process. In the etching process, the sample surface is covered with wax, to prevent it from the etchant (the quantum well, InGaAs and AlGaAs, are etched by HCl), and mounted on the substrate holder. The holder with sample attached is then dipped into HCl until indium is removed. Then, the sample is lapped with SiC powder to decrease its

thickness. Practically, the lower limit of the reduced thickness is around 150-200  $\mu\text{m}$  to prevent the substrate from cracking when holding. When the lapping process is finished, the wax on the sample surface is cleaned by boiling in trichloroethylene, rinsing in acetone and de-ionized water. The sample is cleaved into 200-1000  $\mu\text{m}$  cavity length.

## 4.2 Measurement setup

### 4.2.1 Photoluminescence measurement

Photoluminescence is one of the most sensitive and nondestructive ways to characterize semiconductor materials. The information of material is collected from the light spectrum emitted from the material which results from external light excitation.

When samples are exposed to the exciting photons, the photons are absorbed and excess electron-hole pairs are generated. The highest carrier concentration region is near the illuminated surface. Hence, in order to return to thermal equilibrium state, these carriers would have to diffuse from that region and recombine, radiatively or non-radiatively. The spectrum contains the information of the material such as energy gap, and impurity levels, both donor and acceptor, etc. For quantum well and superlattice structures, interface roughness is also characterized by photoluminescence spectrum.

In this experiment, the photoluminescence method is used as a tool to gauge the quality of the quantum well structures grown before the fabrication of the optical cavity. The measurement setup is shown in Fig. 4.7.

The external light source, an argon laser with a wavelength of 4880  $\text{\AA}$ , is passed through a light chopper and focused onto the sample which is mounted to sample holder in a cryostat with a temperature-controlled feature. In order to receive the large amount information of radiative recombination, the sample is necessary to be cooled to the cryogenic temperature.

The photoluminescence spectra are collected by lens and then optionally passed through the monochromator and detected by the photomultiplier. The measured signal from photomultiplier is sent to the lock-in amplifier that receives the reference signal from the light chopper. Noise from the measured signal is minimized.

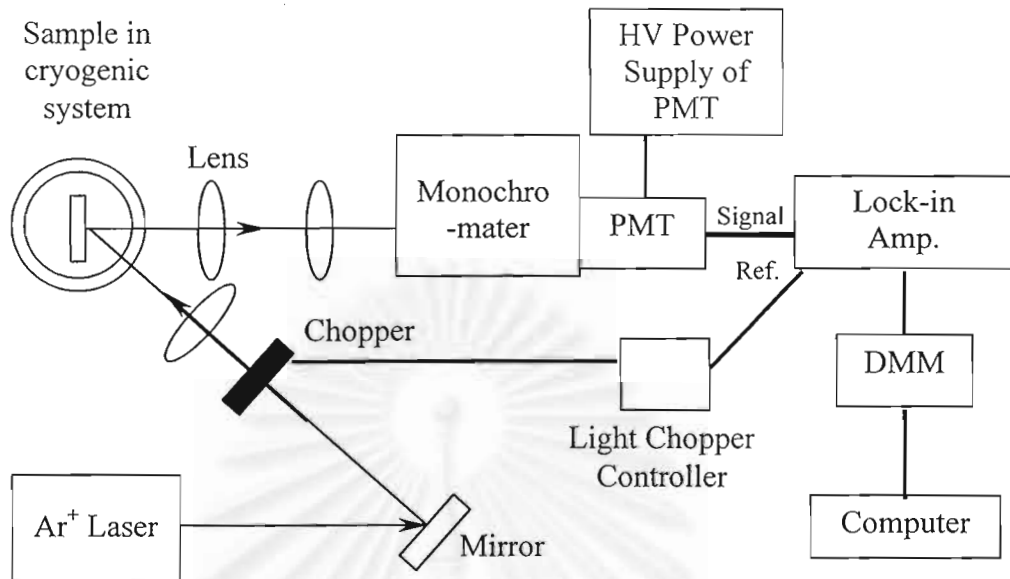


**Fig. 4.6** Photoluminescence measurement setup

#### 4.2.2 Optically pumped measurement

The optically pumped method is the simplest way to create a population inversion condition (see details in Chapter 3) in a material which can result in stimulated emission, the basic phenomena of laser operation. The cleaved facets at the edge of the sample are expected to be the mirrors of the Fabry-Perot cavity providing the selective amplification.

Generally, the optically pumped measurement setup is the same as the photoluminescence process but require a higher power excitation source. However, because of the high measured signal and for practical measurement setup, the lock-in amplifier can be removed from the system without the effect on the desired information.

The argon laser with a wavelength of  $5140 \text{ \AA}$  is focused onto the surface of the cleaved samples which is being cooled to  $77 \text{ K}$  by liquid nitrogen. The focus spot radius is approximately  $50\text{-}100 \text{ }\mu\text{m}$ . The front and side view spectra are collected by the optical power meter optionally passing through the monochromator. In this experiment, the  $1\text{-nm}$  resolution was used. The experiment setup is shown in Fig. 4.7.

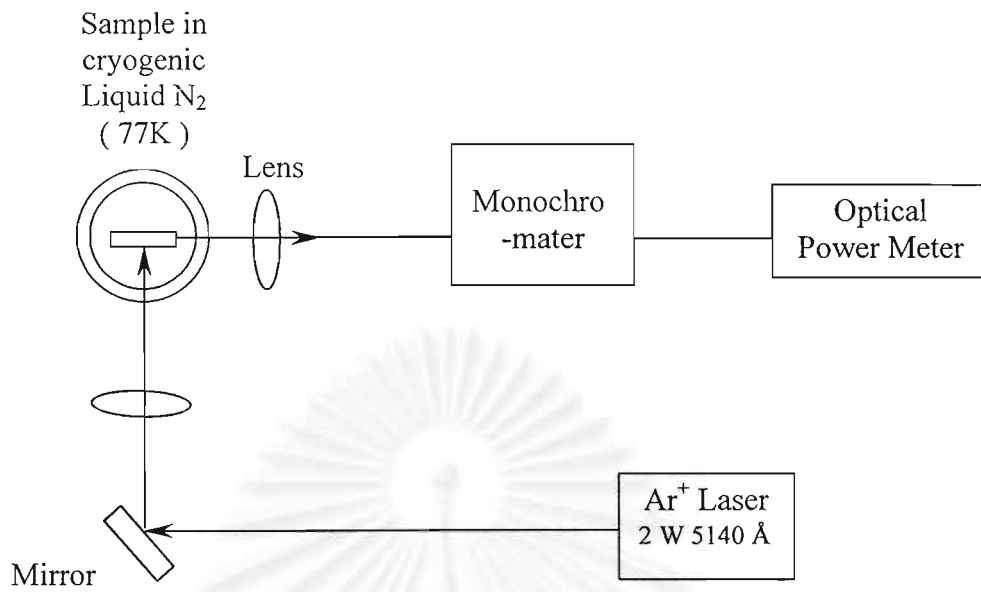


**Fig. 4.7** Size view edge emission optically pumped measurement

### 4.3 Conclusion

This chapter details the growth, the fabrication, and the measurement setup. Figure 4.8 below concludes the processes involved in the experiment.

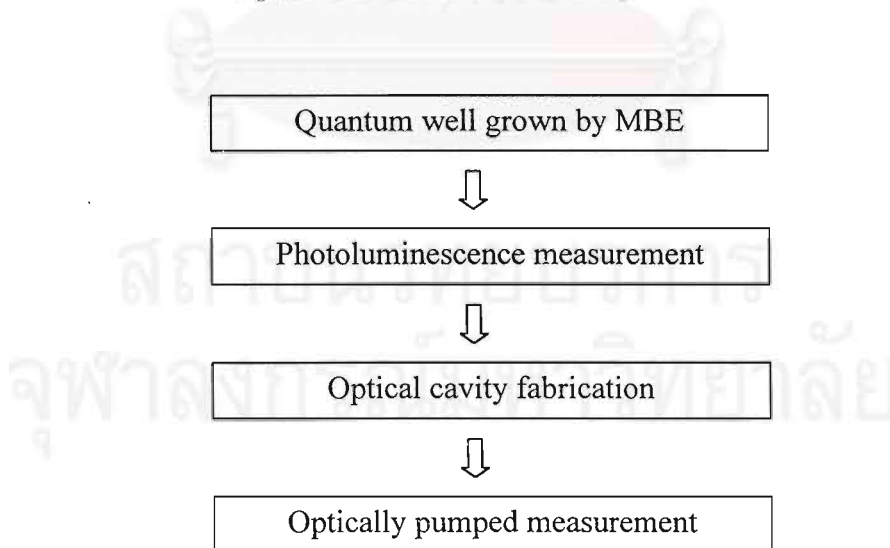


**Fig. 4.8** The process in this experiment

## CHAPTER 5

### Results and Discussion

#### 5.1 Introduction

This chapter is reserved for the result reported from optically pumped technique, which is a modification of photoluminescence measurement as discussed in chapter 4. The spectrum shape and the varying maximum peak with the pumping power from the  $\text{In}_x\text{Ga}_{1-x}\text{As}/\text{GaAs}$  and  $\text{GaAs}/\text{Al}_x\text{Ga}_{1-x}\text{As}$  SQW and MQW are demonstrated and discussed in details.

#### 5.2 Photoluminescence

As described in Chapter 4, the photoluminescence measurement is a useful method to evaluate the quantum structures fabricated in this thesis. The important parameter used to represent the quality of fabricated quantum structure is the spectrum broadening, which is demonstrated by the **full width at half maximum (FWHM)**.

The broadening generally comes from two mechanisms: **homogeneous** and **inhomogeneous** broadening mechanism [28]. The former is due to phonon interaction linearly depending on temperature (in case of acoustic phonon) while the latter arises from localized strain, impurity density variations, alloy clustering, interface roughness in heterostructure and quantum wells. As a result of step-like density of states in quantum well, the spectrum from quantum wells would be narrower than that from bulk semiconductors. However, the interface roughness and other factors would broaden the spectrum from quantum wells. Thus, we can evaluate the interface quality of the quantum well structures fabricated in this thesis from the photoluminescence method.

Fig. 5.1 shows the photoluminescence spectra from the samples, which have the same designed structure. The broad spectrum indicates that the layers are fabricated under undesired conditions which cause interface roughness. We expect that two maximum intensity of this broad spectrum are resulted from unequal thickness of the quantum well layer. However, only the result from photoluminescence measurement can not give us all characterizations of grown layers. The other important measurement, which represents the quality, the thickness, the defect characterization, and etc. is **transmission electron microscopy (TEM)**.



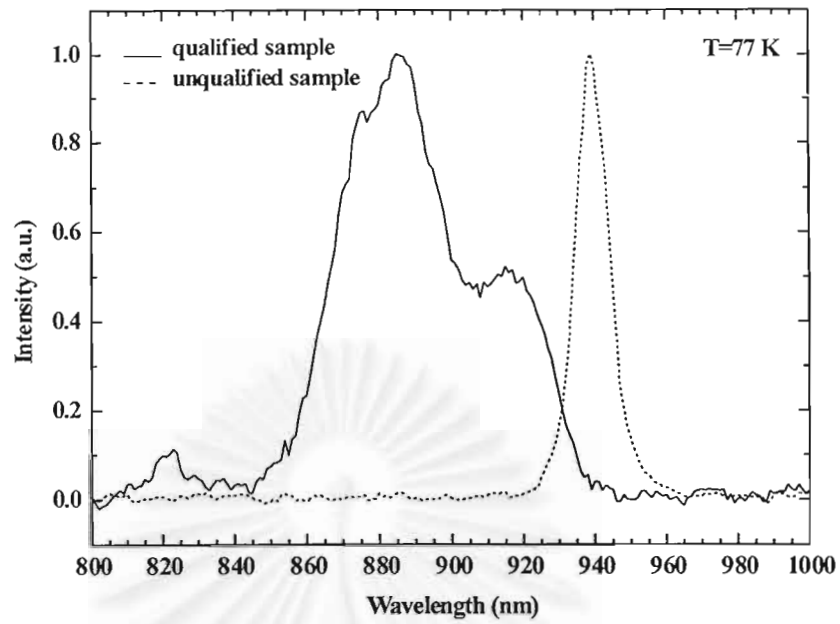


**Fig. 5.1** Photoluminescence spectra from  $\text{In}_{0.2}\text{Ga}_{0.8}\text{As}/\text{GaAs}$  3 MQW with 75 Å well width at 77 K

- **$\text{GaAs}/\text{Al}_x\text{Ga}_{1-x}\text{As}$  quantum well structure**

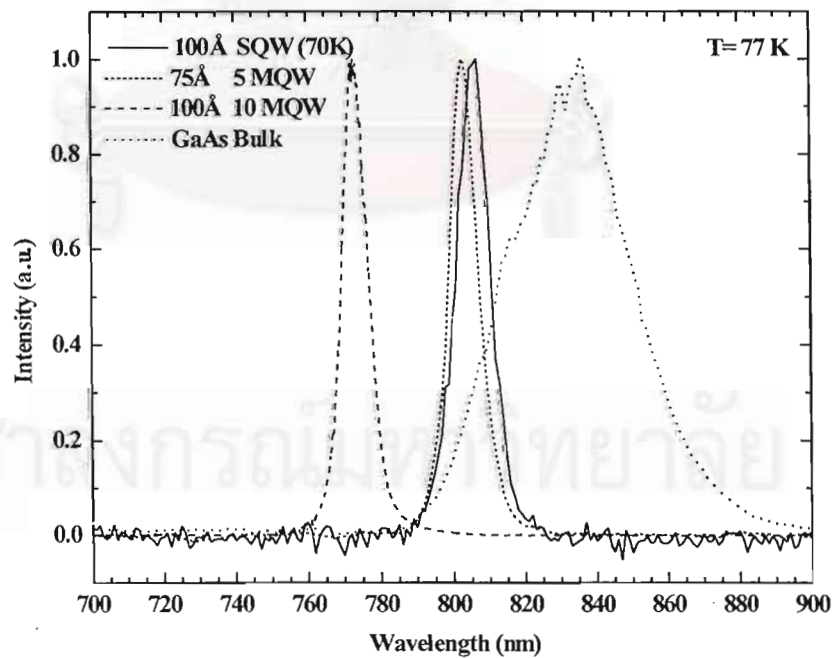


**Fig. 5.2** Photoluminescence spectra from  $\text{GaAs}/\text{Al}_x\text{Ga}_{1-x}\text{As}$  quantum well structures at 70 and 77 K



The photoluminescence spectra from GaAs/Al<sub>0.2</sub>Ga<sub>0.8</sub>As quantum well structures as presented in Chapter 4 are shown in Fig. 5.2. The spectra shape determined by FWHM are stated in Table 5.1 compared with GaAs bulk. The narrow spectrum shape is as a consequence of the step-like density of states of quantum well.

**Table 5.1** The FWHM of photoluminescence spectrum from GaAs/Al<sub>0.2</sub>Ga<sub>0.8</sub>As quantum well structure at 77 K

Well width (Å)	FWHM (nm)
**100 (SQW)	10.4
100 (MQW)	8.00
75 (MQW)	9.00
GaAs Bulk	40.0

\*\* Measured at 70 K

The calculation results compared with the experiment result are indicated in Table 5.2. As discussed in Chapter 2, quantum wells that have the same well depth, one with narrower well width would emit shorter wavelength (higher the effective energy gap). However, in the experiment, quantum well with 75Å well width emits rather longer wavelength (lower effective energy gap) than that with 100 Å well width. This deviation comes from the fact that GaAs/AlGaAs samples are fabricated from various groups as stated in Chapter 4. Thus, the dissimilar conditions used in fabrication processes effect to the grown layer. Although the experiment results diverge from the theory, they are still in an acceptable range.

**Table 5.2** Comparison between calculation and experiment result of Al<sub>0.2</sub>Ga<sub>0.8</sub>As/GaAs SQW and MQW at 77 K and 70 K.

Well width	Calculation		Experiment		% correction	
	Energy level (eV)	Wavelength (nm)	Energy level (eV)	Wavelength (nm)	Energy level	Wavelength
100 Å (SQW)	1.54344**	803.399**	1.537**	807**	0.42%	0.45%

\*\* Measured at 70 K

**Table 5.2** (continued) Comparison between calculation and experiment results of GaAs/ $\text{Al}_{0.2}\text{Ga}_{0.8}\text{As}$  SQW and MQW at 77 K and 70 K.

Well width	Calculation		Experiment		% Correction	
	Energy level (eV)	Wavelength (nm)	Energy level (eV)	Wavelength (nm)	Energy level	Wavelength
*100 Å (10MQW)	1.54177	804.27	1.604	773	4.04%	3.89%
*75 Å (5MQW)	1.55838	795.70	1.544	803	0.92%	0.92%
GaAs Bulk	1.50749	822.56	1.483	836	1.62%	1.63%

*\*The barrier thickness in MQW is wide enough to prevent coupling between each well.*

- **$\text{In}_x\text{Ga}_{1-x}\text{As}/\text{GaAs}$  quantum well structure**

The  $\text{In}_{0.2}\text{Ga}_{0.8}\text{As}/\text{GaAs}$  quantum well structures fabricated in this experiment are SQW, 3 MQW, and 5 MQW. The details of the structure are demonstrated in chapter 4. The photoluminescence spectra from the system in Fig. 4.6 are shown in Fig. 5.2.

As discussed in Chapter 2 that, if the barrier separating each well is greater than 50 Å, the individual well is largely uncoupled and the property of MQW and SQW are quite similar. This theory can be proved by the spectrum shown in Fig. 5.2 from SQW, 3 MQW and 5 MQW with 75 Å well width (400 Å barrier for MQW). These spectra are slightly different in shape, determined by FWHM (Table 5.1), and in wavelengths, providing the maximum intensity (Table 5.2).

For 30 Å well width SQW, the wavelength which is equal to 876 nm gives the maximum intensity. This wavelength which is quite shorter than that of 75 Å well width (the higher effective energy gap) is resulted from the smaller indium content and narrower well width. The former provides the higher energy gap of the well layer and the latter pushes the first quantized state up to the higher energy level.

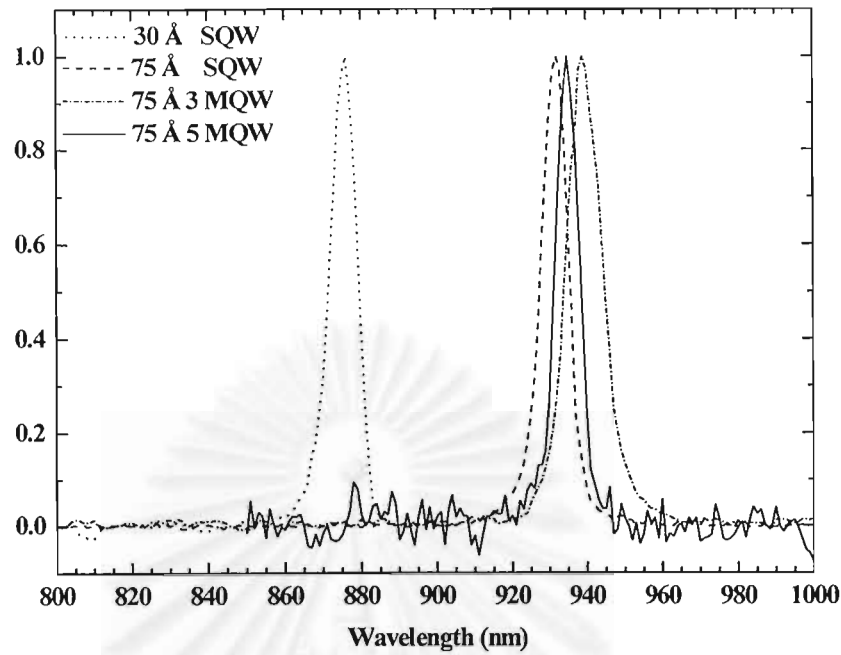


**Fig. 5.3** Photoluminescence spectrum from  $\text{In}_{0.2}\text{Ga}_{0.8}\text{As}/\text{GaAs}$  quantum well structures at 77 K

**Table 5.3** The FWHM of photoluminescence spectra from  $\text{In}_{0.2}\text{Ga}_{0.8}\text{As}/\text{GaAs}$  quantum well structure at 77 K

Well width (Å)	FWHM (nm)
30 (SQW)	8.2
75 (SQW)	8.5
75 (3 MQW)	11.0
75 (5 MQW)	8.0

The wavelengths at maximum intensity emitted from quantum well are lower than the approximated values from Chapter 2 (the effective energy gap is higher). The comparisons are demonstrated in Table 5.4.

**Table 5.4** Comparison between calculation and experiment result of  $\text{In}_{0.2}\text{Ga}_{0.8}\text{As}/\text{GaAs}$  SQW and MQW at 77 K.

Well width	Calculation		Experiment		% correction	
	Energy level (eV)	Wavelength (nm)	Energy level (eV)	Wavelength (nm)	Energy level	Wavelength
30 Å (SQW)	1.33169	931.15	1.415	876	6.25%	5.92%
75 Å (SQW)	1.23193	1006.55	1.330	932	7.96%	7.41%
*75 Å (3MQW)	1.23193	1006.55	1.321	939	7.23%	6.71%
*75 Å (5MQW)	1.23193	1006.55	1.326	935	7.64%	7.11%

\* Assume the barrier thickness in MQW is enough to prevent coupling between each well.

The differences between calculation and measurement come from the inappropriate approximation for strain effect in quantum well structure and the fabrication errors. A general model used for strained degenerate band case is derived by Luttinger and Kohn [20]. This model modifies the effective mass equation to include the strain interaction between degenerate band as detail in ref. [20].

The InGaAs fabrication problems are resulted from the indium content and layer thickness control. From the photoluminescence measurement, the indium content from fabricated samples seems to be smaller than expected owing to the indium desorption. The excessively high growth temperature is responsible for this case. As a consequence of indium desorption, a fewer number atoms adsorb to substrate surface then cause the thinner grown layer which effect the quantized state of quantum well structures.

To know exactly what happen to the fabricated layer, the TEM measurement should be performed. When thickness and the wavelength giving maximum intensity are known, the indium content can be easily predicted (the degree of the correctness depend on the approximating model.).

### 5.3 Optically pump

The qualified samples are put into Fabry-Perot cavity by the preparation process in Chapter 4. The edge emission spectra from side view of the samples and the maximum intensity varied with pumping power are detected by the measurement system shown in Chapter 4. and demonstrated in two sections below.

#### 5.3.1 GaAs/Al<sub>0.2</sub>Ga<sub>0.8</sub>As quantum well structures

- GaAs/Al<sub>0.2</sub>Ga<sub>0.8</sub>As SQW with 100 Å well width (Fig. 5.4)

As shown in Fig. 5.4 (a), the maximum intensity which locates at 804 nm at 77 K, is linearly increasing with pumping power and the spectrum shapes at different pumping power in Fig. 5.4 (b) are the same. Thus, we can interpret that the optical gain is smaller than the losses in this structure.

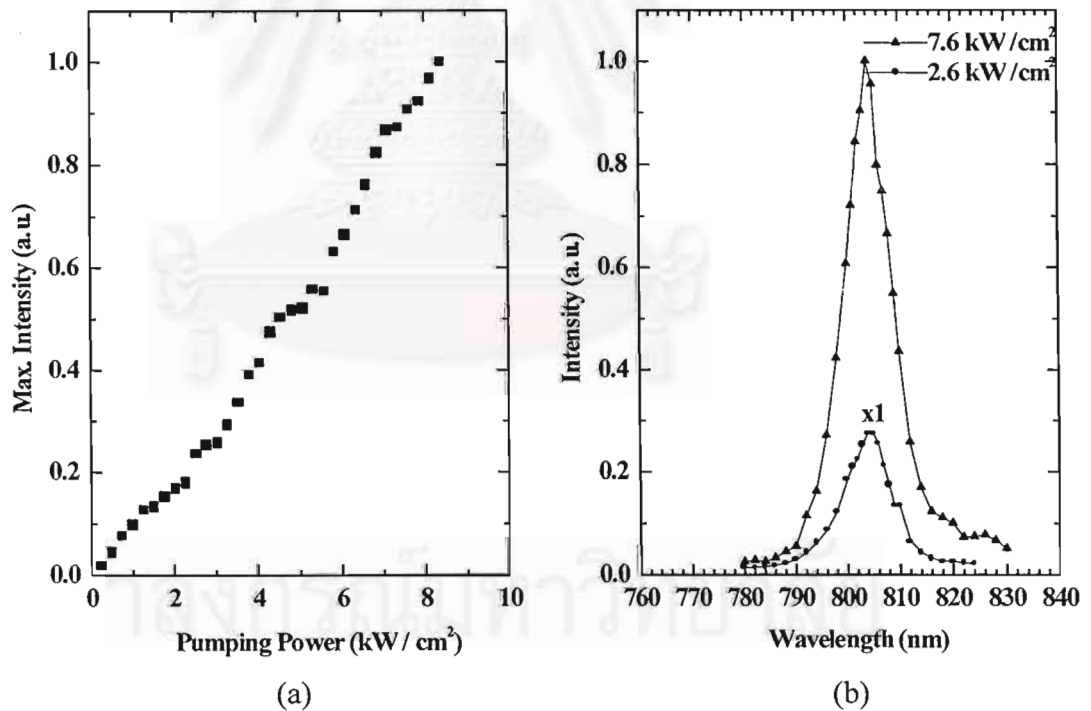


**Fig. 5.4** GaAs/Al<sub>0.2</sub>Ga<sub>0.8</sub>As SQW (a) The variation of the maximum intensity with various pumping power. (b) The side view spectra at 2.6 and 7.6 kW/cm<sup>2</sup>.



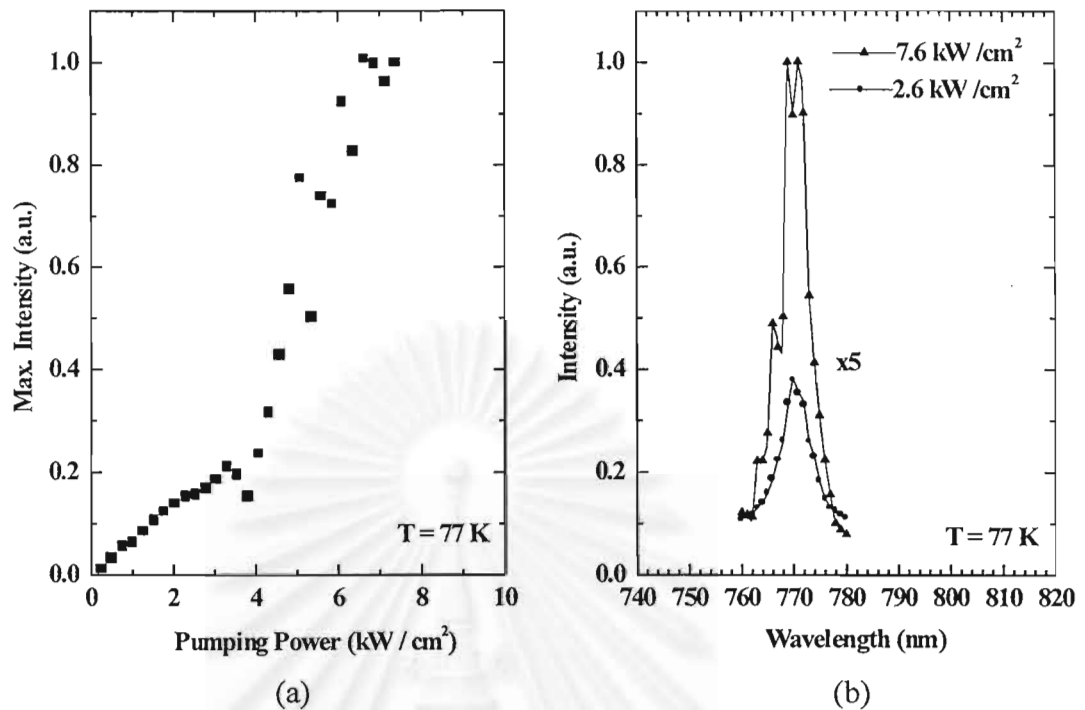


**Fig. 5.5** GaAs/Al<sub>0.2</sub>Ga<sub>0.8</sub>As 10MQW (a) The variation of the maximum intensity with various pumping power. (b) The side view spectra at 2.6 and 7.6 kW/cm<sup>2</sup>

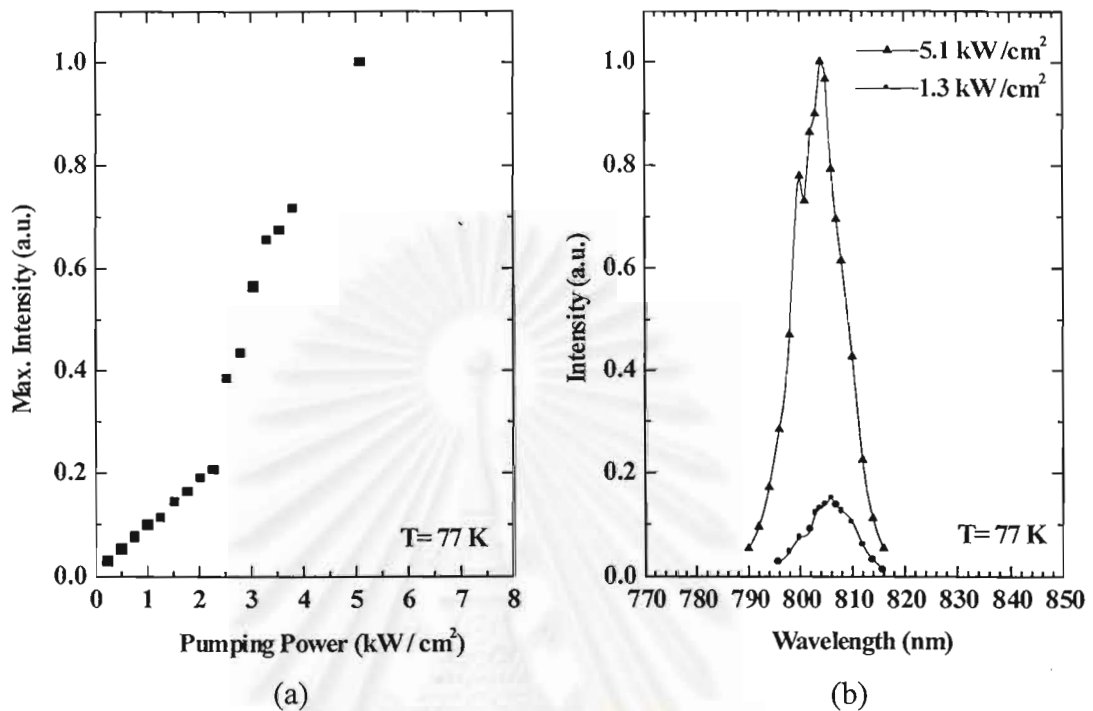
- GaAs/Al<sub>0.2</sub>Ga<sub>0.8</sub>As 10 MQW with 100 Å well width (Fig. 5.5)

Fig. 5.5 (a) shows that the maximum intensity of edge emission spectra grow superlinearly with the pumping power. The change of increasing rate at 4 kW/cm<sup>2</sup> arises from that the increasing optical gain exceeds the existing loss. From Fig 5.5 (b) the spectrum shape at 7.6 kW/cm<sup>2</sup> (above threshold) is slightly narrower than that of 2.6 kW/cm<sup>2</sup> (below threshold). Due to the limit resolution, the exact spectra shape can not be collected. If the high-resolution monochromator is used, the selective amplification is expected to be observed. However, we can conclude that this result is the onset of the stimulated emission.

In this experiment, the maximum intensity was investigated only at 770 nm. As shown in Fig 5.5 (b), the intensity at some pumping power above 4 kW/cm<sup>2</sup> drops. This is because the wavelength at maximum intensity was not kept at fixed value but slightly varied with pumping power.



- *GaAs/Al<sub>0.2</sub>Ga<sub>0.8</sub>As 5 MQW with 100 Å well width and cladding layer(Fig. 5.6)*



**Fig. 5.6** GaAs/Al<sub>0.2</sub>Ga<sub>0.8</sub>As 5 MQW with waveguide (a) The variation of the maximum intensity with various pumping power. (b) The side view spectra at 1.3 and 5.1 kW/cm<sup>2</sup>

Although the identical spectra shapes are collected at 5.1 kW/cm<sup>2</sup> and 1.3 kW/cm<sup>2</sup> (Fig. 5.6 (b)), the maximum intensity shows superlinearly increasing with pumping power and the increasing rate alters at 2.5 kW/cm<sup>2</sup> as shown in Fig. 5.6 (a).

Among these three structures in the experiment, the GaAs/Al<sub>0.2</sub>Ga<sub>0.8</sub>As 5 MQW with waveguide is expected to be the highest efficiency active layer of semiconductor lasers. Although the 10 MQW structure shows the lasing probability, the threshold carrier density is larger than GaAs/Al<sub>0.2</sub>Ga<sub>0.8</sub>As 5 MQW with waveguide because of the combination of the higher confinement factor value and the lower transparency carrier density of GaAs/Al<sub>0.2</sub>Ga<sub>0.8</sub>As 5 MQW. On the other hand, there is no gain possibility in GaAs/Al<sub>0.2</sub>Ga<sub>0.8</sub>As SQW. The reason is that although a fewer number of wells in MQW result in a lower transparency carrier density, the active thickness is also responsible for the optical gain. Thus, the gain of GaAs/Al<sub>0.2</sub>Ga<sub>0.8</sub>As SQW is lower and can not exceed the existing loss.

### 5.3.2 $\text{In}_{0.2}\text{Ga}_{0.8}\text{As}/\text{GaAs}$ quantum well structures

- $\text{In}_{0.2}\text{Ga}_{0.8}\text{As}/\text{GaAs}$  SQW with 75 Å well width (Fig. 5.7)

For  $\text{In}_{0.2}\text{Ga}_{0.8}\text{As}/\text{GaAs}$  75 Å SQW case, in Fig. 5.7 (a) shows the possibility that the maximum intensity would superlinearly increase if the pumping power were higher. The spectrum shape is obviously similar with various pumping powers.

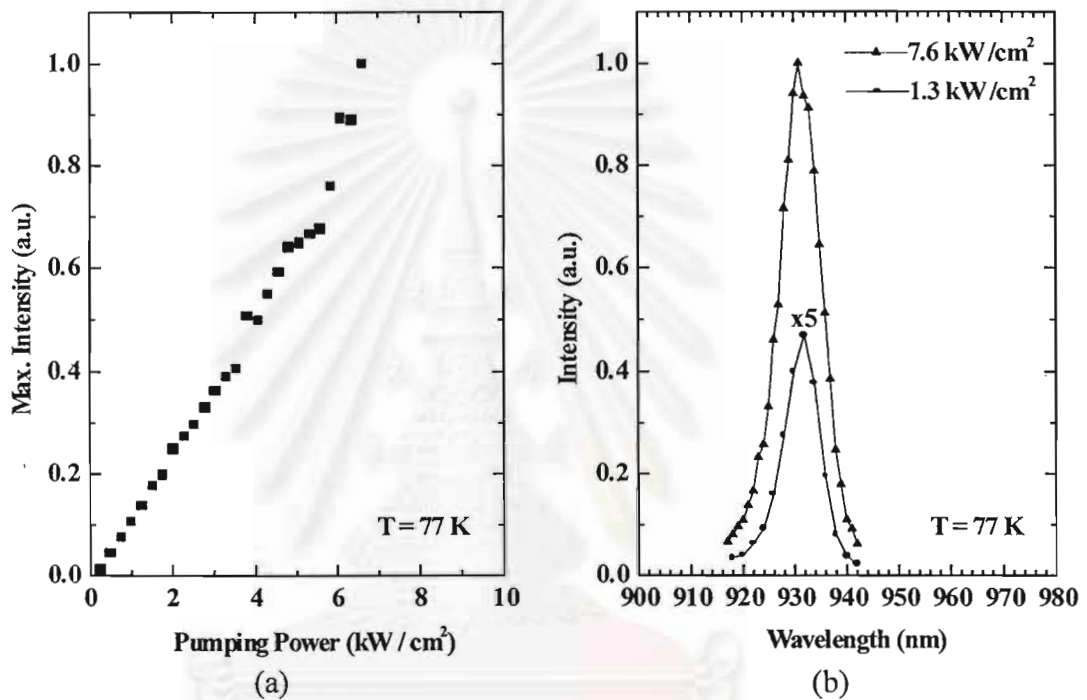
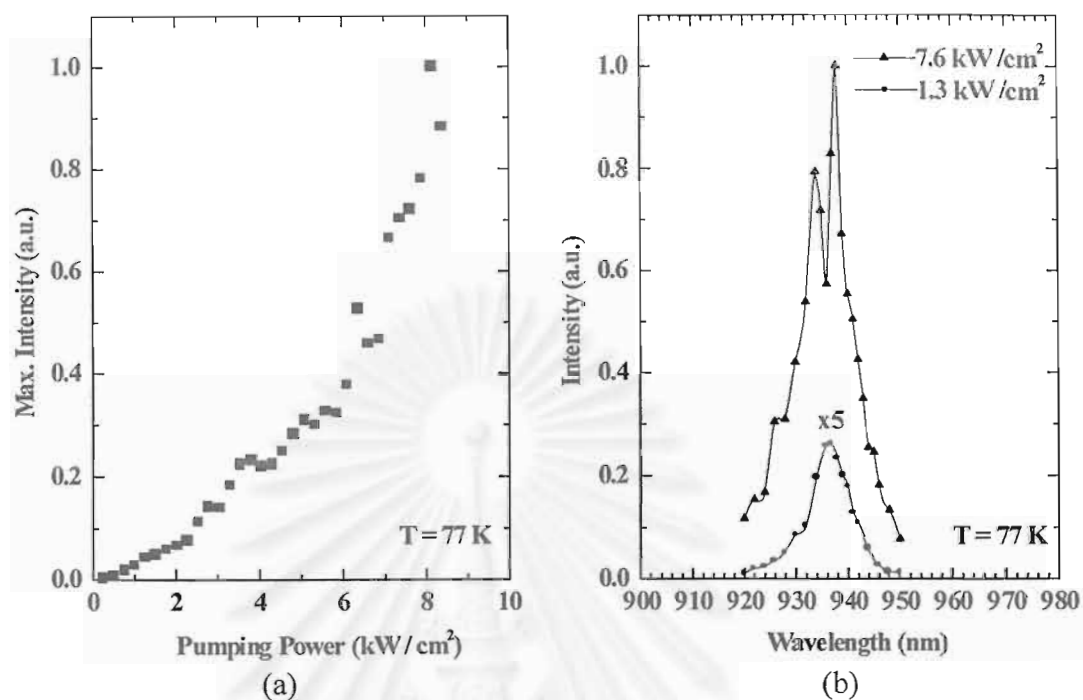


Fig. 5.7  $\text{In}_{0.2}\text{Ga}_{0.8}\text{As}/\text{GaAs}$  SQW (a) The variation of the maximum intensity with various pumping power. (b) The side view spectra at 1.3 and 7.6 kW/cm<sup>2</sup>

- $\text{In}_{0.2}\text{Ga}_{0.8}\text{As}/\text{GaAs}$  3 MQW with 75 Å well width (Fig. 5.8)

The intensity variation of  $\text{In}_{0.2}\text{Ga}_{0.8}\text{As}/\text{GaAs}$  3 MQW demonstrated in Fig. 5.7 (a) is unlike  $\text{GaAs}/\text{Al}_{0.2}\text{Ga}_{0.8}\text{As}$  MQW case. As a result of the unsuitable  $\text{In}_{0.2}\text{Ga}_{0.8}\text{As}$  and  $\text{GaAs}$  refractive index for the optical confinement, the optical loss is expected to occur in an active region. However, thanks to the thickness of active layer, the possibility of stimulated emission can be noticed.

The spectra shape at 7.6 kW/cm<sup>2</sup> shown Fig. 5.7 (b) is supposed to be inaccurately collected owing to the limit resolution.



**Fig. 5.8**  $\text{In}_{0.2}\text{Ga}_{0.8}\text{As}/\text{GaAs}$  3 MQW (a) The variation of the maximum intensity with various pumping power. (b) The side view spectra at 1.3 and 7.6  $\text{kW}/\text{cm}^2$ .

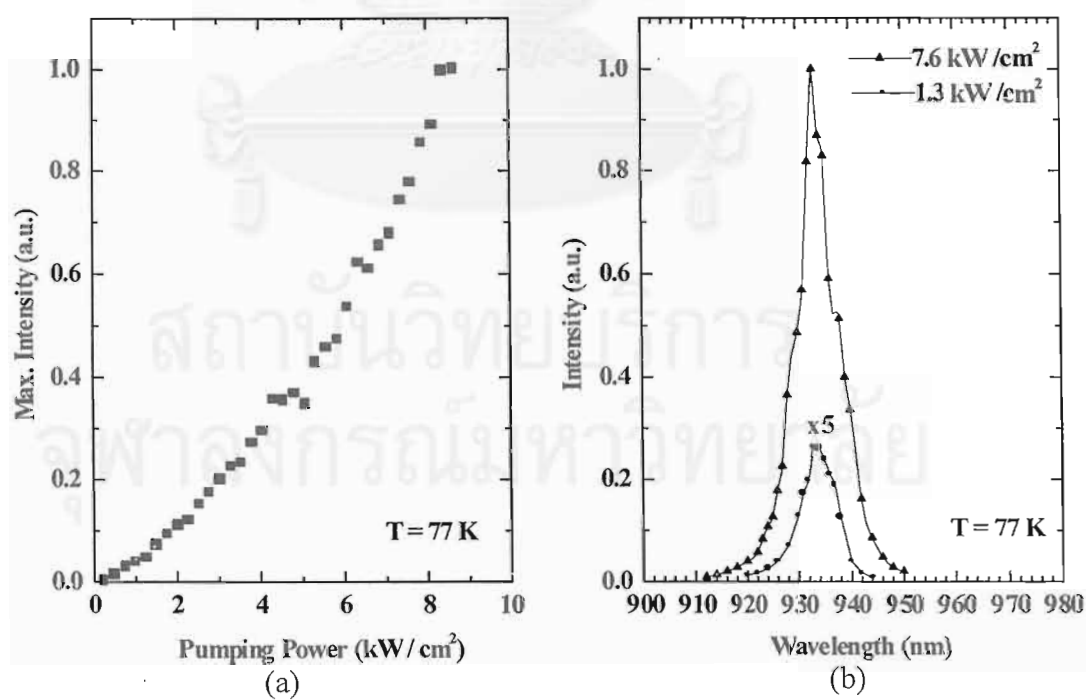


**Fig. 5.9**  $\text{In}_{0.2}\text{Ga}_{0.8}\text{As}/\text{GaAs}$  5 MQW (a) The variation of the maximum intensity with various pumping power. (b) The side view spectra at 1.3 and 7.6  $\text{kW}/\text{cm}^2$

- *In<sub>0.2</sub>Ga<sub>0.8</sub>As/GaAs 5 MQW with 75 Å well width (Fig. 5.9)*

The variation intensity from In<sub>0.2</sub>Ga<sub>0.8</sub>As/GaAs 5 MQW is quite similar to GaAs/In<sub>0.2</sub>Ga<sub>0.8</sub>As 3 MQW (shown in Fig. 5.9 (a)) that there is the possibility of stimulated emission whether there is some optical loss in active layer.

### 5.3.2 Comparison for 2 systems: GaAs/Al<sub>0.2</sub>Ga<sub>0.8</sub>As and In<sub>0.2</sub>Ga<sub>0.8</sub>As/GaAs

For SQW case, the GaAs/Al<sub>0.2</sub>Ga<sub>0.8</sub>As 100 Å well width and the In<sub>0.2</sub>Ga<sub>0.8</sub>As/GaAs 75 Å well width were investigated. The same side view spectra shape and the linearly increasing of maximum intensity with the pumping power reveal that the gain occurring in the SQW structure can not exceed the losses. Owing to the thin active layer of SQW, which can not effectively confine the optical wave in active region, the threshold pumping power of this structure would increase. Another reason is that the gain in SQW is low; thus, the optical gain in SQW can not overcome the loss and no stimulated emission occurs.

On the other hand, MQW structures, both GaAs/Al<sub>0.2</sub>Ga<sub>0.8</sub>As and In<sub>0.2</sub>Ga<sub>0.8</sub>As/GaAs system, demonstrate the possibility of stimulated emission, which is the fundamental mechanism in laser operation. The increasing of maximum intensity with the pumping power of In<sub>0.2</sub>Ga<sub>0.8</sub>As/GaAs 3 MQW and 5 MQW reveal that there is the optical leakage in these structures as a result of unsuitable waveguide (discussed in Chapter 3).

Though the SQW confinement factor is quite poor, In<sub>0.2</sub>Ga<sub>0.8</sub>As/GaAs SQW emits high intensity because the lattice mismatch between In<sub>0.2</sub>Ga<sub>0.8</sub>As and GaAs results in the strain in the grown layer. This causes the reducing hole effective mass which gives the better efficiency of the recombination (see Chapter 2).

To produce the high radiative recombination and to improve the optical confinement, the waveguide with suitable refractive index should be included to quantum structures.

## CHAPTER 6

### Conclusion

The optical spectra emitted from quantum structures were investigated. The side view spectra of MQW structures, both GaAs/Al<sub>0.2</sub>Ga<sub>0.8</sub>As and In<sub>0.2</sub>Ga<sub>0.8</sub>As/GaAs, are superlinearly increasing with the pumping power. In the GaAs/Al<sub>0.2</sub>Ga<sub>0.8</sub>As MQW structure, the threshold pumping power can be clearly observed opposing to In<sub>0.2</sub>Ga<sub>0.8</sub>As/GaAs case. Moreover, the waveguide layers result in the reduction of the threshold pumping power. On the other hand, as a consequence of thin active layer, this phenomenon in SQW can not be noticed in this thesis because the low optical gain can not exceed the existing loss.



จุฬาลงกรณ์มหาวิทยาลัย



## REFERENCES

- [1] M. I. Nathan, W. P. Dumke, G. Burns, F. H. Dill, Jr., and G. Lasher, "Stimulated emission of radiation from GaAs p-n junctions," *Appl. Phys. Lett.*, vol. 1, pp. 62-64, 1962.
- [2] H. Kressel, J. K. Butler, *Semiconductor Lasers and Heterojunction LEDs*, London: Academic, 1977.
- [3] M. A. Herman, H. Sitter, *Molecular Beam Epitaxy Fundamentals and Current Status*, Berlin: Springer-Verlag, 1989.
- [4] C. H. Henry, "The origin of quantum wells and the quantum well laser," in *Quantum Wells Lasers*, P. S. Zory, Ed. New York: Academic, 1993, FOREWORD, pp. 1-16.
- [5] W. T. Tsang, "Quantum confinement heterostructure semiconductor lasers," in *Semiconductors and Semimetals*, vol. 24, New York: Academic, 1987, ch. 7.
- [6] H. Morkoç, B. Sverdlov, and G.-B. Gao, "Strained layer heterostructure, and their applications to MODFET's, HBT's, and lasers," *Proc. IEEE*, vol. 81, no. 4, pp. 493-556, Apr. 1993.
- [7] N. Holonyok, Jr., and M. H. Lee, "Photopumped III-V semiconductor lasers," in *Semiconductors and Semimetals*, vol. 14, New York: Academic, 1979, ch. 1.
- [8] J. I. Pankove, *Optical Processes in Semiconductors*, London: Prentice-Hall, 1971.
- [9] R. M. Kolbas, N. G. Anderson, W. D. Laidig, Y. Sin, Y. C. Lo, K. Y. Hsieh, and Y. J. Yang, "Strained-layer InGaAs-GaAs-AlGaAs photopumped and current injection lasers," *IEEE J. Quantum Electron.*, vol. 24, no. 8, pp. 1605-1613, Aug. 1988.
- [10] P. L. Gourley, J. P. Hohimer, and R. M. Biefeld, "Lasing transitions in GaAs/GaAs<sub>1-x</sub>P<sub>x</sub> strained-layer superlattices with x = 0.1-0.5," *Appl. Phys. Lett.*, vol. 47, pp. 552-554, 1985.
- [11] K. B. Ozanyan, J. E. Nicholls, M. O'Neill, L. May, J. H. C. Hogg, W. E. Hagston, B. Lunn, and D. E. Ashenford, "Room temperature UV lasing from photopumped ZnCdS/ZnS quantum wells," pp. 7/1-7/4, 1996.



- [12] P. Rees, J. F. Heffernan, F. P. Logue, J. F. Donegan, C. Jordon, J. Hegarty, F. Hiei, and A. Ishibashi, "High temperature gain measurements in optically pumped ZnCdSe-ZnSe quantum wells," *IEE Proc. Optoelectron.*, vol. 143, no. 1, pp. 110-112, Feb. 1996.
- [13] M. C. Larson, M. Kondow, T. Kitatani, Y. Yazawa, and M. Okai, "Room temperature continuous-wave photopumped operation of 1.22  $\mu\text{m}$  GaInNAs/GaAs single quantum well vertical-cavity surface-emitting laser," *Electron. Lett.*, vol. 33, no. 11, pp. 959-960, May 1997.
- [14] D. Lee, A. M. Johnson, J. E. Zucker, C. A. Burrus, R. D. Feldman, and R. F. Austin, "High-temperature quasi-continuous operation of optically pumped CdZnTe/ZnTe multiple-quantum-well lasers at 620 nm," *IEEE Photonics Tech. Lett.*, vol. 4, no. 9, pp. 949-951, Sep. 1992.
- [15] E. H. Aifer, W. W. Bewley, C. L. Felix, I. Vurgaftman, L. J. Olafsen, J. R. Meyer, H. Lee, R. U. Martinelli, J. C. Connolly, A. R. Sugg, and G. Olsen, "CW operation of 3.4  $\mu\text{m}$  optically-pumped type-II W laser to 220K," *Electron. Lett.*, vol. 34, no. 16, pp. 1587-1588, Aug. 1998.
- [16] L. A. Coldren, and S. W. Corzine, *Diode Lasers and Photonic Integrated Circuits*, New York: John Wiley & Sons, 1995.
- [17] J. Singh, *Physics of Semiconductor and Their Heterostructures*, Singapore: McGraw-Hill, 1993.
- [18] D. J. Griffiths, *Introduction to Quantum Mechanics*, New York: Prentice-Hall, 1994.
- [19] J. H. Davies, *The Physics of Low-Dimensional Semiconductors: An Introduction*, Cambridge University Press, 1999.
- [20] S. W. Corzine, R.-H. Yan, and L. A. Coldren, "Optical gain in III-V bulk and quantum well semiconductors," in *Quantum Wells Lasers*, P. S. Zory, Ed. New York: Academic, 1993, ch. 1, pp. 17-96.
- [21] P. Bhatattacharya, *Semiconductor Optoelectronic Devices*, 2nd edn., New Jersey: Prentice-Hall, 1993.
- [22] J. Singh, *Semiconductor Optoelectronics Physics and Technology*, Singapore: McGraw-Hill, 1995.
- [23] R. Symms, and J. Cozens, *Optical Guided Waves and Devices*, London: McGraw-Hill, 1993.

- [24] G. P. Agrawal, N. K. Dutta, *Semiconductor Lasers*, Van Nostrand Reinhold, 1993
- [25] S. Adachi, Eds, *Properties of Aluminium Gallium Arsenide*, IEE, INSPEC, 1993.
- [26] W. W. Chow, S. W. Koch, *Semiconductor-Laser Fundamentals Physics of the Gain Material*, Springer-Verlag, 1999
- [27] S. M. Sze, Eds, *Modern Semiconductor Device Physics*, John Wiley & Sons, Inc., 1998
- [28] MBE 32 Operator's Guide Instruction Manual, RIBER, 1991.
- [29] K. Ploog, "Molecular beam epitaxy of artificially layered semiconductor structures—basic concept and recent achievements," in *Physics, Fabrication, and Applications of Multilayered Structures*, P. Dhez and C. Weisbuch, Eds., Nato ASI Series., 1988.
- [30] K. Ploog, L. Tapfer, *Physics and Technology of Semiconductor Quantum Devices*, Springer-Verlag, 1993
- [31] K.-Y. Cheng, "Molecular beam epitaxy technology of III-V compound semiconductors for optoelectronic applications," *IEEE Proc.*, vol. 85, no. 11, pp. 1694-1714, Nov. 1997.
- [32] A. Y. Cho, "Morphology of epitaxial growth of GaAs by a molecular beam method: the observation of surface structures," *J. Appl. Phys.*, vol. 41, no. 7, pp. 2780-2786, Jun. 1970.
- [33] A. Y. Cho, "GaAs epitaxy by a molecular beam method: observations of surface structure on the (001) face," *J. Appl. Phys.*, vol. 42, no. 1, pp. 2074-2080, Apr. 1971.
- [34] B. Goldstein, and D. Szostak, "Preferential evaporation of In from  $\text{Ga}_x\text{In}_{1-x}\text{As}$ ," *Appl. Phys. Lett.*, vol. 26, no. 12, pp. 685-687, Jun. 1975.
- [35] D. J. Arent, S. Nilsson, Y. D. Galeuchet, H. P. Meier, and W. Walter, "Indium adatom migration during molecular beam epitaxial growth of strained InGaAs/GaAs single quantum wells," *Appl. Phys. Lett.*, vol. 55, no. 25, pp. 2611-2613, Dec. 1989.
- [36] H. Wang, T. Fan, J. Wu, Y. Zeng, J. Dong, and M. Kong, "Effects of growth temperature on highly mismatched InAs grown on GaAs substrates by MBE," *J. Cryst. Growth*, vol. 186, pp. 38-42, 1998.

- [37] L. R. Brovelli, D. J. Arent, H. Jaekel, and H. P. Meier, "Indium migration and controlled lateral bandgap variations in high-power strained layer InGaAs-AlGaAs lasers grown on nonplanar substrates," *IEEE J. Quantum Electron.*, vol. 27, no. 6, Jun. 1991.
- [38] P. Bhattacharya, Eds, *Properties of Lattice-Matched and Strained Indium Gallium Arsenide*, IEE, INSPEC, 1993.



จุฬาลงกรณ์มหาวิทยาลัย

## APPENDIX A

### Calculation Parameters for Quantum Well Structure

All parameters in this appendix are from ref. [25], [38] and reference there in.

- $\text{Al}_x\text{Ga}_{1-x}\text{As}/\text{GaAs}$  system

#### 1. Energy Gap

$$E_{g,\text{GaAs}} = \left( \left( 1.424 + \frac{\alpha_{\text{GaAs}} \cdot (300)^2}{\beta_{\text{GaAs}} + 300} \right) - \frac{\alpha_{\text{GaAs}} \cdot T^2}{T + \beta_{\text{GaAs}}} \right) \text{ eV}$$

$$E_{g,\text{AlGaAs}} = \left( \left( (1.424 + 1.247x) + \frac{\alpha_{\text{AlGaAs}} \cdot (300)^2}{\beta_{\text{AlGaAs}} + 300} \right) - \frac{\alpha_{\text{AlGaAs}} \cdot T^2}{T + \beta_{\text{AlGaAs}}} \right) \text{ eV}$$

Where  $\alpha_{\text{GaAs}} = 5.5 \cdot 10^{-4} \text{ K}^{-1}$ ,  $\beta_{\text{GaAs}} = 225 \text{ K}$ ,  $\alpha_{\text{AlGaAs}} = 6.58 \cdot 10^{-4} \text{ K}^{-1}$ ,  $\beta_{\text{AlGaAs}} = 248 \text{ K}$

$$\frac{\Delta E_C}{\Delta E_V} = \frac{60}{40}$$

#### 2. Effective mass

$$m_{e,\text{Al}_x\text{Ga}_{1-x}\text{As}} = (0.067 + 0.083x) \cdot m_0$$

$$m_{hh,\text{Al}_x\text{Ga}_{1-x}\text{As}} = \frac{1}{(\gamma_1 - 2\gamma_2)} \cdot m_0$$

$$m_0 = 9.109 \cdot 10^{-31} \text{ kg}$$

$$\gamma_{1,\text{Al}_x\text{Ga}_{1-x}\text{As}} = 6.85 \cdot (1-x) + 3.45 \cdot x$$

$$\gamma_{2,\text{Al}_x\text{Ga}_{1-x}\text{As}} = 2.10 \cdot (1-x) + 0.68 \cdot x$$

- $\text{In}_x\text{Ga}_{1-x}\text{As} / \text{GaAs}$  system

#### 1. Energy Gap

$E_{g,\text{GaAs}}$  as in  $\text{GaAs}/\text{Al}_x\text{Ga}_{1-x}\text{As}$

$$E_{g,\text{InGaAs}} = \left( 1.52 - \frac{\alpha_{\text{GaAs}} T^2}{T + \beta_{\text{GaAs}}} \right) + \left( 0.42 - \frac{\alpha_{\text{InAs}} T^2}{T + \beta_{\text{InAs}}} - 1.52 + \frac{\alpha_{\text{GaAs}} T^2}{T + \beta_{\text{GaAs}}} \right) \cdot x - 0.475 \cdot x \cdot (1-x) \text{ eV}$$

Where  $\alpha_{GaAs} = 10.6 \cdot 10^{-4} \text{ K}^{-1}$ ,  $\beta_{GaAs} = 671 \text{ K}$ ,  $\alpha_{InAs} = 2.76 \cdot 10^{-4} \text{ K}^{-1}$ ,  $\beta_{InAs} = 83 \text{ K}$

$$\frac{\Delta E_C}{\Delta E_V} = \frac{60}{40}$$

## 2. Energy Shifting Parameter

lattice constant :  $a_{GaAs} = 5.6533 \text{ \AA}$ ,  $a_{In_xGa_{1-x}As} = (5.6533 + 0.405 \cdot x) \text{ \AA}$

lattice mismatch :  $\varepsilon = \frac{a_{GaAs}}{a_{In_xGa_{1-x}As}} - 1$

Valence band energy shifting [17] :  $\delta = 0.5 \cdot 5.966 \cdot \varepsilon \text{ eV}$

## 3. Effective mass

$$m_{e,In_xGa_{1-x}As} = (0.067 - 0.04x) \cdot m_0$$

$$m_{hh,In_xGa_{1-x}As} = \frac{1}{(\gamma_1 - 2\gamma_2)} \cdot m_0$$

$$m_0 = 9.109 \cdot 10^{-31} \text{ kg}$$

$$\gamma_{1,In_xGa_{1-x}As} = 6.85 \cdot (1 - x) + 19.67 \cdot x$$

$$\gamma_{2,In_xGa_{1-x}As} = 2.10 \cdot (1 - x) + 8.37 \cdot x$$

## LIST OF PUBLICATION

1. Rudeesun Songmuang, Suwat Sopitpan, and Somsak Panyakeow, "Study on Optically Pumped Edge Emission of  $\text{Al}_{0.2}\text{Ga}_{0.8}\text{As}/\text{GaAs}$  10 Multiple Quantum Well and  $\text{GaAs}/\text{In}_{0.2}\text{Ga}_{0.8}\text{As}$  Single Quantum Well," *Proceeding of the 21st conference on electrical engineering, Kasetsart University* (8-9 December 1998)



จุฬาลงกรณ์มหาวิทยาลัย



## BIOGRAPHY

Miss Rudeesun Songmuang was born at 17 March 1976 in Bangkok. She received Bachelor degree of Engineering from Department of Engineering, Faculty of Engineering, Chulalongkorn University and started studying at Semiconductor Device Research Laboratory (SDRL) at Chulalongkorn University in Master degree in 1997.



จุฬาลงกรณ์มหาวิทยาลัย